Contributions to Mineralogy and Petrology (2022) 177:40
https://doi.org/10.1007/s00410-022-01903-y

ORIGINAL PAPER

MafiCH: a general model for H_2O–CO_2 solubility in mafic magmas

Chelsea M. Allison[1,2] · **Kurt Roggensack**[1] · **Amanda B. Clarke**[1,3]

Received: 30 June 2021 / Accepted: 24 February 2022 / Published online: 19 March 2022

Abstract

The solubility of CO_2 in mafic magmas is strongly dependent on magma composition, which ultimately affects magma storage conditions and eruptive behavior. Recent experimental work showed that previously published volatile solubility models for mafic magmas are not well calibrated at mid-crustal pressures (400–600 MPa). Using a simple thermodynamic model, here we construct a general CO_2 solubility model for mafic magmas by establishing the compositional dependence of two key thermodynamic parameters. The model is calibrated using experimental data from 10 magma compositions that span a range of pressures as well as silica (44–53 wt.%) and total alkali (2–9 wt.%) contents. We also survey the experimental literature for relevant H_2O solubility data to determine how to model H_2O solubility for these magmas. We combine these separate CO_2 and H_2O solubility models into a single general model for mixed-fluid (H_2O–CO_2) solubility in mafic magmas called MafiCH. We test the MafiCH model using experiments from three compositions that fall both within and beyond the calibrated range, and find that the model accurately constrains the CO_2 solubility of depolymerized magmas. Sensitivity tests identify that Na, Ca, and Al have the largest effect on CO_2 solubility while Si and Mg do not play a strong role in CO_2 solubility in mafic, depolymerized melts. Overall, saturation pressures calculated using the new model presented here are typically lower than those predicted by previous models. The model provides a new framework to interpret volcanic data from mafic magma compositions for which no experimental data is available.

Keywords Volatile solubility · Basaltic volcanism · Alkali basalts · Experimental petrology · Thermodynamics

Introduction

The solubility of volatiles in magmas plays a critical role in the storage conditions and eventual eruption of magma. At magma storage depths, carbon is the primary volatile element in the exsolved phase because it has a low solubility compared to H_2O and its solubility is very strongly pressure dependent (e.g., Holloway and Blank 1994). Mafic magmas dissolve carbon as carbonate (e.g., Fine and Stolper 1986; Blank and Brooker 1994), and experimental work has shown that mafic magmas with variable alkali contents exhibit a very wide range of CO_2 solubilities (e.g., Dixon 1997; Lesne et al. 2011b; Shishkina et al. 2014; Vetere et al. 2014; Allison et al. 2019). While the compositional dependence of CO_2 solubility in mafic magmas is notable, H_2O solubility does not vary significantly by composition in mafic magmas (e.g., Moore et al. 1998; Lesne et al. 2011a; Iacono-Marziano et al. 2012). Of course, most natural magmas contain a mixed (H_2O–CO_2) volatile phase, so while we focus primarily on CO_2 solubility in this work due to its significant compositional variability, we also assess H_2O solubility in order to model behavior in natural systems.

Knowledge of volatile solubility is required to constrain characteristics of the volcanic plumbing system using pre-eruptive volatile contents (e.g., Lowenstern 1995). It is not typically feasible or reasonable, however, to conduct solubility experiments on an unstudied composition solely to interpret volcanic data. Instead, well-calibrated volatile solubility models can be used to determine these properties in unstudied magma compositions. Numerous models exist (e.g., Newman and Lowenstern 2002; Papale et al. 2006;

Communicated by Mark S. Ghiorso.

✉ Chelsea M. Allison
cmalliso@asu.edu

[1] School of Earth and Space Exploration, Arizona State University, Tempe, AZ 85287-6004, USA

[2] Present Address: Department of Geosciences, Baylor University, Waco, TX 76798, USA

[3] Istituto Nazionale di Geofisica e Vulcanologia, Sezione di Pisa, Via della Faggiola, 32, 56126 Pisa, Italy

Iacono-Marziano et al. 2012; Duan 2014; Shishkina et al. 2014; Ghiorso and Gualda 2015), but it is not always clear which model is most appropriate for the volcanic system of interest (e.g., Wieser et al. 2022). The choice between similar volatile solubility models may ultimately be based on familiarity and ease of use. For example, the VolatileCalc model (Newman and Lowenstern 2002), which uses the basalt model from Dixon (1997), is currently commonly used to calculate fluid-saturated isobars and melt inclusion saturation pressures for basaltic compositions. In the two decades since that model was published, however, additional experiments have provided updated solubility relationships (e.g., experiments on alkali-rich mafic magmas from Botcharnikov et al. 2005, Behrens et al. 2009, Pichavant et al. 2009, Lesne et al. 2011a, b, Iacono-Marziano et al. 2012, Iacovino et al. 2013, Pichavant et al. 2014, Shishkina et al. 2014, Vetere et al. 2014, Iacovino et al. 2016, Allison et al. 2019, and Schanofski et al. 2019).

The applicability of volatile solubility models may be limited as a result of the pressure–temperature–compositional (*P*–*T*–*X*) range of experiments used to calibrate the models, which may partly explain why volatile solubility models can yield drastically different results (e.g., saturation pressures) for a single composition (refer to Wieser et al. 2022 for detailed discussion regarding volatile solubility model differences). For instance, Allison et al. (2019) presented new H_2O–CO_2 experiments in six alkali-rich mafic magmas at pressures from 400 to 600 MPa and found that previously published models did not completely describe the CO_2 results. Allison et al. (2019) instead calibrated individual thermodynamic models for CO_2 solubility that showed strong agreement with the experimental data for each of the six compositions. In Fig. 1, we show the 400 MPa fluid-saturated isobar (at 1200 °C) calculated using two of the Allison et al. (2019) individual models compared with results using six earlier volatile solubility models (colored curves; models described in Table 1). In the Etna composition (Fig. 1a), for a completely anhydrous magma (at $H_2O = 0$ wt%), the models predict a sizeable range of dissolved CO_2 contents from ~ 2500 to ~ 4500 ppm at 400 MPa and 1200 °C. The models show even more disagreement for the Vesuvius composition (Fig. 1b), with calculated dissolved CO_2 contents from ~ 2500 to ~ 9000 ppm at anhydrous conditions. These results illustrate that the selection of volatile solubility model can strongly impact the interpretation of a volcanic system.

In this study, we develop a method to calculate mixed-fluid (H_2O–CO_2) solubility calibrated for a wide range of mafic magma compositions at pressures up to 700 MPa. The model, called MafiCH, can be thought of as a combination of models. For CO_2 solubility, we use a thermodynamic approach adapted from Holloway and Blank (1994) and incorporate the full multicomponent composition into the model to achieve robust solubility relationships. We use experiments from Allison et al. (2019) and additional sources to calibrate the model. H_2O solubility is calculated using an empirical method adapted from Lesne et al. (2011a) based on an evaluation of H_2O solubility models using experimental data from the literature. To test the accuracy and applicability of the MafiCH solubility model, we

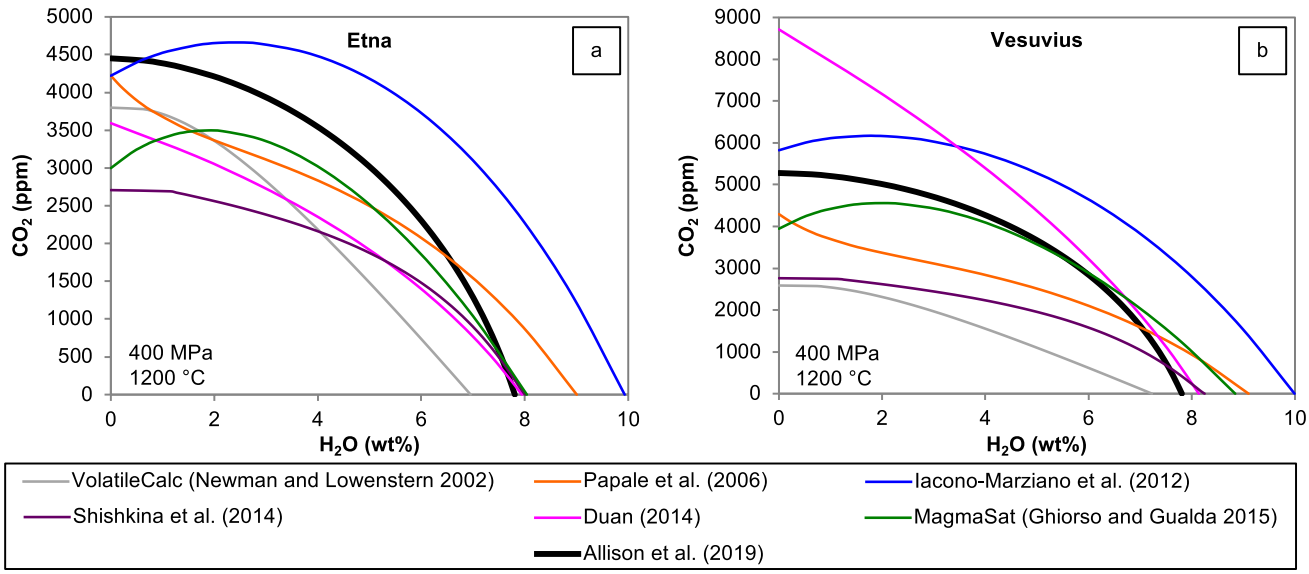

Fig. 1 Comparison of previously published solubility models for mafic magmas. 400 MPa isobars calculated using different models for the (**a**) Etna and (**b**) Vesuvius compositions at 1200 °C. Isobars from Allison et al. (2019) are calculated using the individual thermodynamic models. For models that allow for fO_2 input, Fe speciation was calculated using Kilinc et al. (1983) at NNO + 1 (see supplementary material Table S2)

Table 1 Brief summary of previously published solubility models for mafic magmas that can be applied to alkali-rich compositions

Model	Basis	H_2O effect on CO_2	Tools for Calculations	Suggested[a] P range (MPa)	Suggested[a] T range (°C)	Compositional range	fO_2 Consideration (Fe speciation)
VolatileCalc (Newman and Lowenstern 2002; basalt model based on Dixon 1997)	Simple thermodynamic model; SiO_2 parameterization for solubility at P_0	None	Excel macro spreadsheet[b]*	0–500	1000–1400 for basalt[h]	<49 wt% SiO_2 for basalt	Not specified; requires only wt% SiO_2 input for basalt
Papale Papale (1997), Papale and Polacci (1999), Papale et al. (2006)	Thermodynamic; binary interaction parameters for H_2O and CO_2; elements TiO_2, MnO, P_2O_5 not calibrated	CO_2 solubility increases at lowest H_2O contents	Multiple tools developed after publication[c]	0–1000 (for mixed H_2O—CO_2)	630–1630 (for mixed H_2O—CO_2)	Silicate melts	Accounts for different fO_2 conditions
Iacono-Marziano et al. (2012)	Parameterization of thermodynamic model; inputs: NBO/O, Na_2O+K_2O, $FeO+MgO$, $Al_2O_3/(CaO+K_2O+Na_2O)$	Low H_2O decreases CO_2 solubility	Web calculator[d]*	0–1000	950–1500	Mafic magmas	All Fe as Fe^{+2}
Duan (2014)	Thermodynamic; binary interaction parameters for H_2O and CO_2; elements TiO_2, MnO, P_2O_5 not calibrated	None	.exe for Windows[e]	0–3000	660–1730	Silicate melts	Accounts for different fO_2 conditions
Shishkina et al. (2014)	Empirical model; input: Π* (Ca^{+2}, K^{+1}, Na^{+1}, Fe^{+2}*, Mg^{+2}, Si^{+4}, Al^{+3})	None	Solubility equations in source paper[f]*	50–500	1200–1250[i]	MORB to nephelinite (mafic magmas)	All Fe as Fe^{+2}
MagmaSat (Ghiorso and Gualda 2015)	Thermodynamic; binary interaction parameters for H_2O, CO_2, and $CaCO_3$; element MnO not calibrated	Low H_2O decreases CO_2 solubility	.app for Macintosh or web calculator[g]*	0–3000	600–1400	All natural magmas	Accounts for different fO_2 conditions

[a] P–T ranges listed are suggestions from the source articles for each model and in some cases may extend slightly beyond the P–T range of the calibration dataset

[b] VolatileCalc spreadsheet available for download from: https://volcanoes.usgs.gov/observatories/yvo/jlowenstern/other/software_jbl.html

[c] Calculations using Papale model in this study were performed using the web calculator at: http://melts.ofm-research.org/CORBA_CTserver/Papale/Papale.php; also available in Fortran (SOLWCAD program) from http://www.pi.ingv.it/progetti/eurovolc/

[d] Web calculator for Iacono-Marziano model: http://calcul-isto.cnrs-orleans.fr/apps/h2o-co2-systems/

[e] Website listed in Duan (2014) is no longer maintained; .exe was downloaded for this study from http://gcmodel.kl-edi.ac.cn/archives/programs.htm in 2017 (link provided by Duan by personal communication) but this website is also no longer maintained

[f] To calculate mixed-fluid solubility relationships from the Shishkina et al. (2014) equations we determine fluid fugacities and therefore partial pressures using the modified Redlich–Kwong equation of state (Holloway 1977, 1981, 1987) with the Saxena and Fei (1987) high-pressure correction as detailed in the appendix of Holloway and Blank (1994). We first calculate the pure fluid fugacity at the total pressure of the system, then multiply the pure fugacity by the fluid composition, and finally determine the partial pressure from this value of H_2O or CO_2 fugacity using the equation of state

[g] Details for accessing MagmaSat at: http://melts.ofm-research.org/

[h] T dependence in VolatileCalc is not calibrated from experimental data; it is a direct result of the equation of state

[i] The Shishkina et al. (2014) equations do not include a temperature term, but the model is calibrated from experiments conducted at 1200–1250 °C

*Calculations for these models can also be performed using VESIcal (Iacovino et al. 2021)

compare model calculations with experimental data from Fanara et al. (2015) and Schanofski et al. (2019) that were not used in the model calibration. Two of the tested compositions (trachybasalt and leucitite) are largely within the calibrated range of the model, while a third more silicic magma (phonolite) was tested to explore the compositional limits of the model. We next evaluate how the choice of solubility model can impact volcanic interpretation by comparing saturation pressures calculated by different models. Finally, we assess what might control CO_2 solubility in alkali-rich mafic magmas based on insights from this new general model.

Previously published models for H_2O–CO_2 solubility in mafic magmas

Before building a new model, we first examine some of the approaches that have been used to model mixed-fluid (H_2O–CO_2) solubility in mafic compositions. We focus on six solubility models that calculate changes in solubility as a result of compositional variability over a wide range of conditions. The details of the six models examined here, including how they were accessed for this study, are summarized in Table 1.

Broadly speaking, these models vary as a result of how they are constructed and calibrated. First, solubility models are calibrated using experimental data, so the *P–T–X* range for which they are valid depends on the experiments incorporated into each model. Some models are constructed as a result of new experimental data, and thus have a very specific compositional and pressure range. Some other models are comprehensive, in that they constrain volatile solubility for all magmas, from basalt to rhyolite, across a temperature and pressure range that encompasses conditions relevant for most natural systems. The treatment of carbon in comprehensive models is variable, as some models account for the fact that mafic end members dissolve carbon solely as carbonate while felsic magmas store carbon as carbon dioxide. Second, models vary in their mathematical construction, which can range from full multi-component models based in thermodynamics to purely empirical models with single-parameter inputs. One additional manner in which models can vary is in how they are available to users. Options may include applications that are specific to an operating system (i.e., .app for Mac or .exe for Windows), other downloadable file formats such as spreadsheets, or web-based calculators. However, some published models may not include any sort of calculator at all, or the calculator may be missing a desired function (e.g., a method to calculate saturation pressures). Fortunately, the recent publication of open-source tool VESIcal (Iacovino et al. 2021) for Python3 has addressed many of these issues of accessibility for a number of the previously published volatile solubility models.

VolatileCalc (Newman and Lowenstern 2002) is a very commonly used tool for determining H_2O–CO_2 solubility relationships, and it employs the oldest model that we discuss in this work. VolatileCalc is available as an excel macro spreadsheet that incorporates separate solubility models for rhyolitic and basaltic magmas. The model for basalt in VolatileCalc comes from the work of Dixon (1997), in which a simple thermodynamic model (Fine and Stolper 1986; Stolper and Holloway 1988; Dixon et al. 1995) was calibrated using previously published experiments from four mafic compositions. In this approach, major element cation fractions from these compositions were combined into a single parameter called Π, where cations capable of bonding with carbonate (Ca^{+2}, Na^{+1}, K^{+1}, Mg^{+2}, Fe^{+2}) contribute to higher Π values and polymerizing cations (Al^{+3} and Si^{+4}) lower the value of Π. Π was then linearly correlated with CO_2 solubility at a single pressure (100 MPa) to generate a relationship between Π and thermodynamic equilibrium. While applying this model to natural samples, Dixon (1997) found that Π varied linearly with SiO_2 content in glasses from an alkalic ocean island suite, and so SiO_2 content was used as a proxy for Π. This simplified SiO_2-based algorithm of Dixon (1997) was the model incorporated into VolatileCalc (Newman and Lowenstern 2002). While very straightforward to use, this model is restricted to calculation of solubility for magmas with < 49 wt% SiO_2 and is not recommended for use at pressures > 500 MPa.

A more recent model by Iacono-Marziano et al. (2012) provided updated solubility relationships specific to alkali-rich mafic magmas. Iacono-Marziano et al. (2012) presented new experimental data on a trachybasalt composition from Etna volcano, and combined the new data with experiments from the literature to calibrate a volatile solubility model. They generated a multi-parameter fit to thermodynamic expressions to produce a semi-empirical model. The Iacono-Marziano et al. (2012) models for H_2O and CO_2 are largely controlled by a calculated parameter, NBO/O, which had been suggested in previous studies to strongly control CO_2 solubility (e.g., Brooker et al. 2001). NBO refers to non-bridging oxygens, or oxygens associated with network-modifying cations (i.e., oxygens bonded with K^{+1}, Na^{+1}, Ca^{+2}, Mg^{+2}, and Fe^{+2}) rather than polymerizing tetrahedra (i.e., oxygens bonded with Si^{+4}, Ti^{+4}, and Al^{+3}). The CO_2 model from Iacono-Marziano et al. (2012) also requires inputs of FeO + MgO, H_2O, and total alkali content.

Even more recently, Shishkina et al. (2014) conducted experiments across eight different mafic compositions to assess volatile solubility. Like Iacono-Marziano et al. (2012), Shishkina et al. (2014) combined their new experiments with literature data to calibrate a model. The Shishkina et al. (2014) study published purely empirical fits for H_2O and CO_2 solubility at 1200–1250 °C. The Shishkina et al. (2014) equation for CO_2 is an exponential relationship with

an updated Π parameterization, termed Π*, for its compositional factor, while the equation for H_2O is a polynomial fit that depends on the Na + K cation fraction composition of the magma. The Shishkina et al. (2014) study did not provide a recommendation for how to combine the equations for mixed fluid compositions (i.e., how to calculate H_2O and CO_2 partial pressures). The details of how we perform calculations for mixed-fluids using the Shishkina et al. (2014) model in this study (e.g., isobars in Fig. 1) are described in a footnote to Table 1.

The final three volatile solubility models examined here are comprehensive thermodynamic models. The Papale model (Papale 1997; Papale and Polacci 1999; Papale et al. 2006) was one of the first comprehensive H_2O–CO_2 solubility models, while Duan (2014) and MagmaSat (Ghiorso and Gualda 2015) were developed more recently. Each of these models surveyed the experimental literature and used these data to calibrate binary interaction parameters for their thermodynamic models that describe how the volatile species interact with different compositional components in the melt. The main ways these three models vary from one another are the specific experiments that are used to calibrate each model, the equations of state used for the fluids (i.e., determination of fluid fugacity), and how different compositional elements are used in the interaction parameters. For example, both Papale et al. (2006) and MagmaSat (Ghiorso and Gualda 2015) include an influence of H_2O on CO_2 solubility, though Papale et al. (2006) shows higher CO_2 solubility at low H_2O for basalts while MagmaSat (Ghiorso and Gualda 2015) shows the opposite effect. Both Duan (2014) and MagmaSat (Ghiorso and Gualda 2015) use the same equation of state (Duan and Zhang 2006), but differ in other ways, such as the treatment of carbon speciation (CO_3 and CO_2), which is accounted for in MagmaSat (Ghiorso and Gualda 2015) but not Duan (2014).

There are at least three additional models that can be used to constrain volatile solubility in mafic magmas, though we do not examine them in detail for this study for the reasons discussed here. The Lesne et al. (2011a, b) study measured solubility in three alkali-rich compositions, but the CO_2 model is calibrated only at low pressures (< 200 MPa). The Lesne et al. (2011b) experiments were later incorporated into the Allison et al. (2019) individual thermodynamic fits for CO_2 solubility. SolEx (Witham et al. 2012) is a program that uses the Π formulation from Dixon (1997), as well as solubility relationships for other volatile elements (S, Cl). However, it does not include a function to calculate saturation pressure, which is a particularly meaningful way to compare models used in this work. Finally, Eguchi and Dasgupta (2018) is a model that constrains only the solubility of CO_2 at relatively anhydrous compositions, and so it is not relevant for many of the mixed-fluid magmatic systems we discuss here.

The MafiCH model

We construct a new general model, called MafiCH, for calculating H_2O–CO_2 solubility as a function of mafic magma composition. The strength of the new CO_2 model we present in MafiCH comes from its thermodynamic basis, use of the full multicomponent magma composition, and calibration across a wide P-X range within the realm of mafic magmas that dissolve carbon as CO_3. The CO_2 model is calibrated with thermodynamic data from 10 compositionally variable mafic magmas for which a wide pressure range of experimental data are available, including the six compositions from Allison et al. (2019). The full major element composition of these magmas was used to derive a relationship describing the thermodynamic parameters. Our primary focus is on CO_2 solubility, but the solubility of H_2O is critical for the interpretation of natural magmas that typically contain mixed H_2O–CO_2 fluids. Thus, we also explore H_2O solubility in mafic magmas based on the experimental literature and previously published models. Note that an excel spreadsheet is provided in the supplementary material to perform solubility calculations using the model. This spreadsheet does not use macros, so it should be compatible with a range of spreadsheet programs. We also include two Python3 scripts for functions that cannot be calculated in excel without the use of macros: degassing paths and a series of saturation pressures (i.e., for a large dataset). Full details for using these scripts are included in the supplementary material. We test the new MafiCH model against recent experimental data for magma compositions both within and beyond the calibrated compositional range.

CO_2 solubility in mafic magmas

The thermodynamic model for CO_2 solubility in mafic magmas

We use the simple thermodynamic model that was described by Fine and Stolper (1986) and Stolper and Holloway (1988) to constrain the concentration of dissolved carbon in equilibrium with a pure CO_2 fluid. We selected this particular model because numerous studies of CO_2 solubility in mafic magmas (e.g., Holloway and Blank 1994; Thibault and Holloway 1994; Dixon et al. 1995; Lesne et al. 2011b) including Allison et al. (2019) found that the CO_2 solubility data from experiments showed strong agreement with this thermodynamic treatment. Complete details of the model are included in Holloway and Blank (1994) and Allison et al. (2019) and briefly explained here. Note that because the vast majority

of solubility experiments for a single composition are performed at a constant temperature (typically 1200 or 1250 °C for mafic magmas), we do not possess the appropriate data to explore the temperature dependence of this model and thus present the model formulation at a constant temperature.

In this model, because CO_2 is stored in mafic magma as CO_3, CO_2 solubility is defined by the equilibrium of the reaction:

$$CO_2(\text{vapor}) + O^{2-}(\text{melt}) = CO_3^{2-}(\text{melt}). \quad (1)$$

The equilibrium constant (K) of this reaction at pressure P and constant temperature T is given by:

$$K(P,T) = K_0(P_0,T_0) \times \exp\left[-\Delta V_r^{0,m} \times (P - P_0) \times (R \times T)^{-1}\right]. \quad (2)$$

Note that because this model assumes equilibrium with a pure CO_2 fluid, the pressure term in Eq. 2 refers to the partial pressure of CO_2 in the system when dealing with a mixed-fluid (H_2O–CO_2) system. In Eq. 2, K_0 (P_0, T_0) is the equilibrium constant at a reference pressure and temperature. $\Delta V_r^{0,m}$ is the partial molar volume change of the condensed (melt) components of the reaction in Eq. 1 and is considered to be independent of pressure and temperature. Thermodynamic parameters K_0 (P_0, T_0) and $\Delta V_r^{0,m}$ are determined empirically for different magma compositions.

To calculate CO_2 contents from the equilibrium constant K (P, T) determined in Eq. 2, first calculate K_f:

$$K_f = K(P,T) \times f_{CO_2}(P,T), \quad (3)$$

then $X_{CO_3}^m$:

$$X_{CO_3}^m = K_f \times \left(1 - K_f\right)^{-1}, \quad (4)$$

and finally wt% CO_2:

$$\text{wt\% } CO_2 = \left(44.01 \times X_{CO_3}^m\right) \times \left\{\left(44.01 \times X_{CO_3}^m\right) + \left[\left(1 - X_{CO_3}^m\right) \times FW_{\text{one}}\right]\right\} \quad (5)$$

In Eq. 5, 44.01 is the formula weight of CO_2 (in g mol^{-1}) and FW_{one} is the formula weight of the magma on a one-oxygen basis; for alkali basalt the value of FW_{one} is 36.594 g mol^{-1} (Holloway and Blank 1994). In this work we treat FW_{one} as a constant value since it does not vary significantly for mafic magmas; values of FW_{one} for the 10 compositions we use to calibrate our general model are within ± 1.4 g mol^{-1} of the alkali basalt value.

The thermodynamic parameters $\Delta V_r^{0,m}$ and K_0 (P_0, T_0) can be determined for different compositions from a linear regression of experimental data (i.e., Fig. 10 in Allison et al. 2019). On a plot with $\ln\left[f_{CO_2}(P,T) \times \left(X_{CO_2}^m\right)^{-1}\right]$ versus $\left[\left(P - P_0\right) \times (R \times T)^{-1}\right]$, where $X_{CO_2}^m$ is the mole fraction of dissolved CO_2, the slope of a linear regression through experiment data yields $\Delta V_r^{0,m}$ and the y-intercept corresponds to $-\ln K_0$. As explained above, P refers to the partial pressure due to CO_2 for a mixed-fluid experiment. Note that the values of $\ln\left[f_{CO_2}(P,T) \times \left(X_{CO_2}^m\right)^{-1}\right]$ will differ based on the units of pressure used for the fugacity term. This difference will be a constant value for every experiment data point: the natural logarithm of the conversion between pressure units (i.e., values using MPa = ln (0.1) + values using bars). However, the value of $\left[\left(P - P_0\right) \times (R \times T)^{-1}\right]$ does not vary by pressure units since the value of the gas constant R will also change to account for different units. Consequently, the y-intercept and therefore K_0 will change depending on what pressure units are used, but $\Delta V_r^{0,m}$ depends only on the volume unit used for R.

The previous studies that have used this model published $\ln K_0$ values determined from pressure in bars, so we also use units of bars for calculations to maintain legacy consistency and then convert to SI units of MPa. In this work the reference conditions are 1000 bars (i.e., 100 MPa) and 1200 °C. The presence of the gas constant R necessitates that temperature be in units of Kelvin for calculations. Thus, the value of R used throughout this work is 83.144621 cm^3 bar K^{-1} mol^{-1}, and the units of $\Delta V_r^{0,m}$ are cm^3 mol^{-1}.

Figure 2 shows the effect of the thermodynamic parameters on CO_2 solubility. More negative values of $\ln K_0$ correlate with lower CO_2 solubilities for the same value of $\Delta V_r^{0,m}$. $\Delta V_r^{0,m}$ changes the curvature of the solubility curve such that larger values of $\Delta V_r^{0,m}$ result in lower CO_2 solubilities at pressures greater than P_0 for the same value of K_0. Changes in K_0 and $\Delta V_r^{0,m}$ have greater impact on CO_2 solubility as CO_2 fugacity increases. For the reasons described above, values of $\ln K_0$ shown in Fig. 2 were calculated using pressure in bars, and the solubility curve results were then converted to MPa.

This thermodynamic model requires information about the properties of the fluid (i.e., an equation of state) to perform calculations, even for a pure CO_2 system. We use the modified Redlich–Kwong equation of state (Holloway 1977, 1981, 1987) with the Saxena and Fei (1987) high-pressure correction as detailed in the appendix of Holloway and Blank (1994). Because the thermodynamic model is calibrated by correlating CO_2 solubility with CO_2 fugacity (see Fig. 2), any volatile solubility calculations made using the model presented in this study must use this same equation of state (modified Redlich–Kwong with high-pressure correction). This equation of state is internally consistent with this simple thermodynamic model, and it is specifically calibrated in the P–T region of interest for crustal magmas. One of the

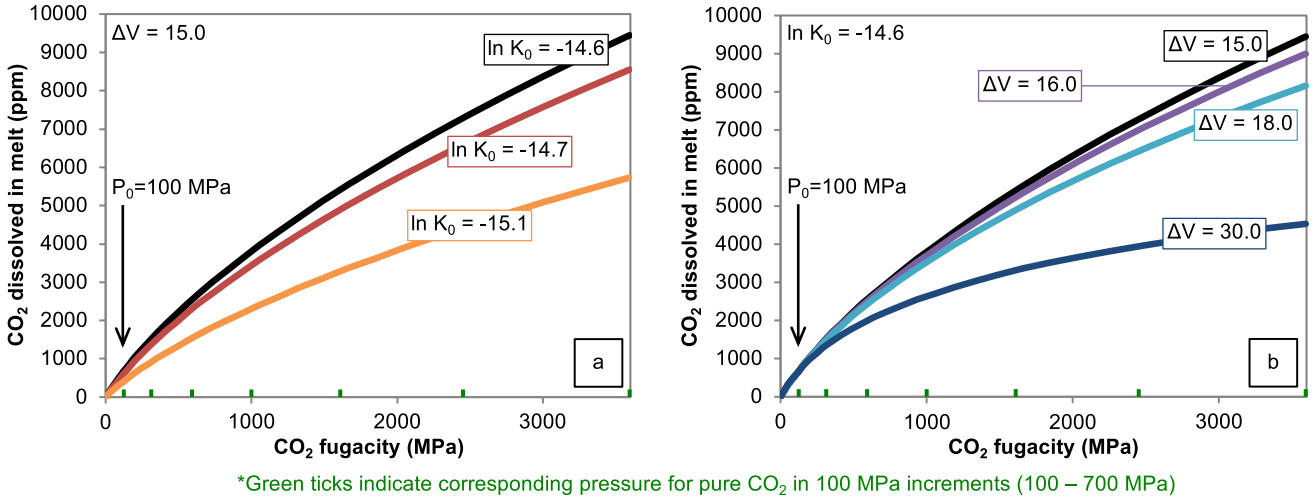

Fig. 2 Impact of the thermodynamic parameters on CO_2 solubility. Properties of the CO_2 fluid (plotted on the *x*-axis) required for calculation of the curves are determined using the modified Redlich–Kwong equation of state (Holloway 1977, 1981, 1987) with the Saxena and Fei (1987) high-pressure correction as detailed in the appendix to Holloway and Blank (1994). **a** At constant value of $\Delta V_r^{0,m}$ decreasing $\ln K_0$ values correlate with lower CO_2 solubilities. **b** At constant value of K_0 increasing $\Delta V_r^{0,m}$ correlates with lower slope and lower CO_2 solubilities. Note that values of $\ln K_0$ shown here were calculated using pressure in bars to maintain legacy consistency, and the solubility curve results were converted to MPa for the plot

more recent equations of state for H_2O and CO_2 (Duan and Zhang 2006) was designed to be applicable over a very wide range of crustal conditions, and it yields very similar values of pure CO_2 and H_2O fugacity to our selected equation of state (see supplementary material Table S1). For CO_2, these two equations of state begin to diverge slightly only at the highest pressures considered by this study (> 600 MPa), with Duan and Zhang (2006) predicting slightly higher CO_2 fugacities.

Development of a general thermodynamic model for CO_2 solubility in mafic magmas

To produce a general model for CO_2 solubility in mafic magmas, we develop a compositional fit for parameters $\Delta V_r^{0,m}$ and K_0 (P_0, T_0) (as $\ln K_0$) in the thermodynamic model (see Eq. 2). To ensure a wide compositional range for this model, we calibrate this general model using the six compositions from Allison et al. (2019), which also incorporated experimental data from Iacono-Marziano et al. (2012) and Lesne et al. (2011b), as well as four additional compositions from the experimental literature (see Table 2 and supplementary material Table S2). We selected these 10 compositions not only for their compositional diversity, but also because the available experiments were conducted over a wide pressure range (including experiments ≥ 500 MPa) and had well-constrained fluid compositions, particularly at low $X_{H_2O}^f$.

From the literature, we incorporate experiments from a basanite (Holloway and Blank 1994), leucitite (Thibault and Holloway 1994), basalt (N72 from Shishkina et al. 2010), and phonotephrite (AH3 from Vetere et al. 2014). The basanite and leucitite experiments were both previously used by Dixon (1997) to define Π, and contain lower SiO_2 than the compositions studied by Allison et al. (2019). We include the basalt (N72) experiments from Shishkina et al. (2010) to extend the compositional range of the model to lower total alkali contents. The phonotephrite composition (AH3) from Vetere et al. (2014) contains high total alkali contents (~9 wt%), with different proportions of Na_2O and K_2O compared to the high-alkali compositions from Allison et al. (2019), in addition to higher SiO_2.

The compositional variability of the 10 magmas used to calibrate the general model for CO_2 is shown in Fig. 3. The magmas encompass a wide range of compositions, from 44 to 53 wt% SiO_2 and 2 to 9 wt% total alkalis ($Na_2O + K_2O$; Fig. 3a). The compositions not only show a wide range of silica and total alkali contents, but also different relative proportions of each alkali component. Importantly, the compositions also vary significantly in the other major elements (Fig. 3b). In Fig. 3b, the relative cation fractions of each composition are plotted compared to the Etna composition. No two compositions follow the same pattern in major element composition. For example, while the Sunset Crater composition shares similar Si^{+4}, Ti^{+4}, Al^{+3}, and Fe^{+2}* contents to the Etna composition, the two magmas vary in Mg^{+2} and Ca^{+2}. The Stromboli and SFVF compositions follow similar trends in Ti^{+4}, Al^{+3}, and Fe^{+2}*, but SFVF has higher

Table 2 Thermodynamic parameters, $\Delta V_r^{0,m}$ and $\ln K_0$ for each composition with associated cation fractions used to construct the general model for CO_2

Composition	$\Delta V_r^{0,m}$	$\ln K_0$[a]	$\ln K_0$[b]	Si^{+4}	Ti^{+4}	Al^{+3}	Fe^{+2}*	Mg^{+2}	Ca^{+2}	Na^{+1}	K^{+1}
Compositions from Allison et al. (2019)											
Sunset Crater	16.40	− 14.67	− 12.37	0.439	0.012	0.176	0.085	0.119	0.097	0.061	0.009
SFVF	15.02	− 14.87	− 12.57	0.490	0.008	0.189	0.061	0.081	0.091	0.061	0.018
Erebus	15.83	− 14.65	− 12.35	0.439	0.019	0.205	0.080	0.046	0.069	0.108	0.033
Vesuvius	24.42	− 14.04	− 11.74	0.452	0.007	0.167	0.063	0.092	0.115	0.035	0.069
Etna	21.59	− 14.28	− 11.98	0.440	0.013	0.177	0.081	0.093	0.113	0.063	0.020
Stromboli	14.93	− 14.68	− 12.38	0.451	0.006	0.183	0.063	0.107	0.123	0.044	0.023
Compositions from other studies											
Basanite[c]	21.72	− 14.32	− 12.02	0.423	0.022	0.165	0.092	0.124	0.081	0.077	0.016
Leucitite[d]	21.53	− 13.36	− 11.06	0.407	0.019	0.139	0.070	0.126	0.141	0.057	0.041
AH3 phonotephrite[e]	30.45	− 13.26	− 10.96	0.447	0.006	0.161	0.057	0.079	0.106	0.123	0.021
N72 Basalt[f]	19.05	− 14.86	− 12.56	0.466	0.006	0.200	0.073	0.097	0.113	0.042	0.003

Note that only the elements listed in this table are included when normalizing cation fractions (i.e., phosphorus and manganese are not included)

[a]$\ln K_0$ for pressure in bars; these values were used to calibrate Eq. 7

[b]$\ln K_0$ for pressure in MPa for comparison

[c]Basanite composition from Holloway and Blank (1994)

[d]Leucitite composition from Thibault and Holloway (1994)

[e]AH3 Phonotephrite composition from Vetere et al. (2014)

[f]N72 Basalt composition from Shishkina et al. (2010)

*Fe^{+2} calculated from total iron expressed as FeO

Na^{+1} and lower Mg^{+2} and Ca^{+2} content than Stromboli. This strong variability in the calibration compositions serves to generate a robust model that can predict CO_2 solubility in numerous mafic magmas.

The thermodynamic parameters $\Delta V_r^{0,m}$ and K_0 (P_0, T_0) have already been determined for eight of these compositions in the original publications of those experiments. Values of $\Delta V_r^{0,m}$ and K_0 (P_0, T_0) were calibrated in Allison et al. (2019) for all six compositions in that study, in Holloway and Blank (1994) for the basanite, and in Thibault and Holloway (1994) for the leucitite. Here we calibrate values of $\Delta V_r^{0,m}$ and K_0 (P_0, T_0) for the N72 basalt (Shishkina et al. 2010) and AH3 phonotephrite (Vetere et al. 2014) using the linear regression method described in the previous subsection for inclusion in this model.

We used the following criteria to select experiments from the N72 basalt (Shishkina et al. 2010) and AH3 phonotephrite (Vetere et al. 2014) to generate the regressions for the thermodynamic parameters $\Delta V_r^{0,m}$ and K_0 (P_0, T_0). First, all pure H_2O experiments from both compositions and four experiments in Shishkina et al. (2010) without successful fluid composition determinations were excluded by necessity. Second, we excluded experiments with $X_{H_2O}^f$ values below 0.1. These studies determined fluid composition by the mass loss method, and for $X_{H_2O}^f$ values below 0.1, there is only a very small mass of H_2O in the fluid (generally < 0.1 mg), so any uncertainty in this measurement can yield large errors in fluid compositions (see supplementary material). Third, we also excluded some experiments with very low values of $\left[\left(P-P_0\right)\times(R\times T)^{-1}\right]$, because the parameter determination method does not perform well at very low partial pressures of CO_2 (Holloway and Blank 1994). In particular, experiments with low $\left[\left(P-P_0\right)\times(R\times T)^{-1}\right]$ values and CO_2 abundances below ~ 175 ppm were targeted for exclusion. The experiments used to calibrate the thermodynamic parameters for AH3 (Vetere et al. 2014) and N72 (Shishkina et al. 2010) are listed in the supplementary material (Table S3).

To produce compositional relationships for the thermodynamic parameters ($\Delta V_r^{0,m}$ and $\ln K_0$), we use a multiple linear regression of cation fractions (Table 2) from each composition. Note that because oxygen fugacity is not always measured in experimental or natural samples, we calculate cation fractions with all iron as FeO (Fe^{+2}). Also, because the reporting of phosphorus and manganese is inconsistent in the literature, these elements are not included in the normalization of cation fractions. A series of multiple linear regressions yielded the following best-fit compositional relationships:

$$\Delta V_r^{0,m}=\beta+\sum\left(\alpha_i\times D_i\right) \tag{6}$$

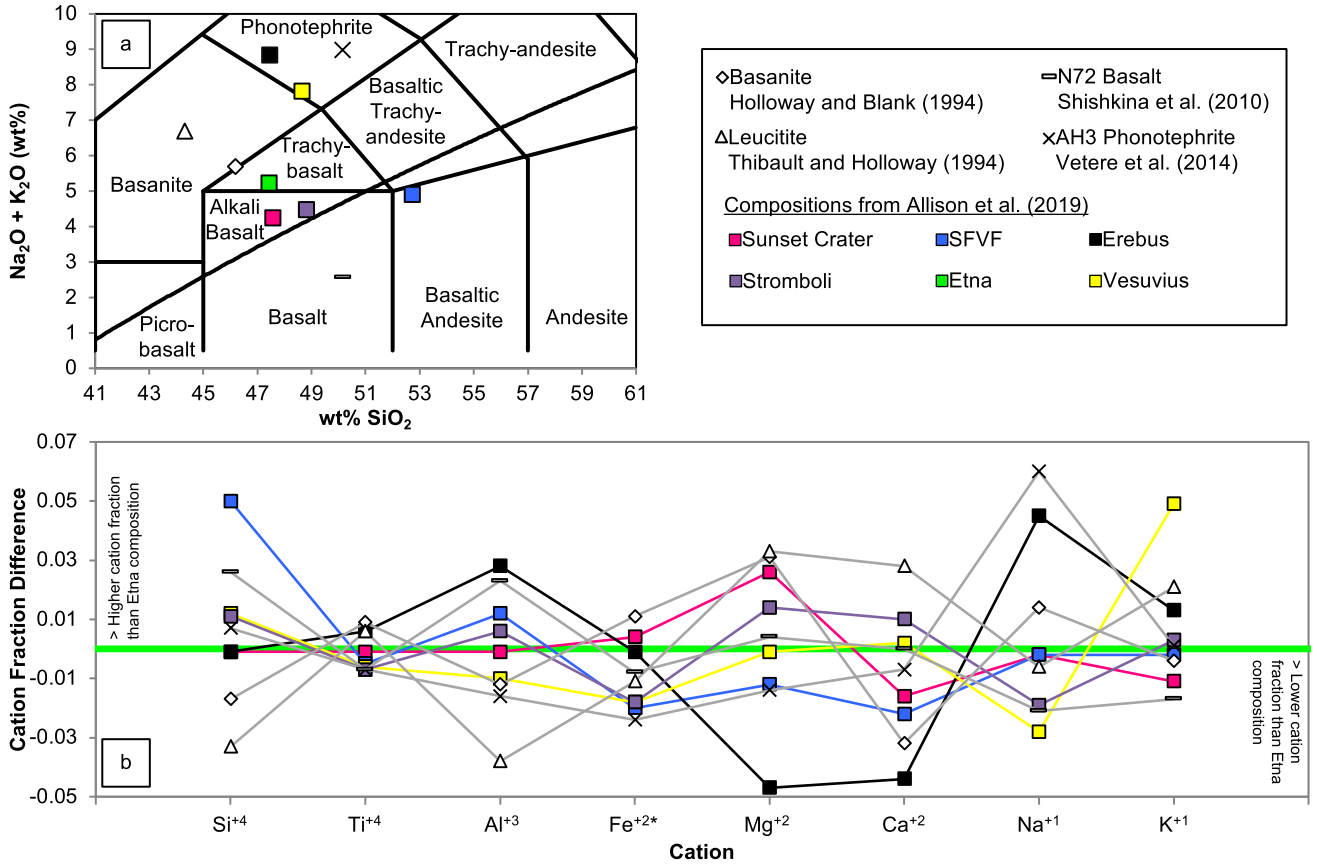

Fig. 3 Compositions included in the general model for CO_2. **a** Total alkali and silica compositions of experiments. **b** Cation fractions of each composition as referenced to the Etna composition

Table 3 Coefficients for $\Delta V_r^{0,m}$ equation

i	α_i value	Standard error	p value
$Si^{+4} + Na^{+1}$	3375.552	±322.351	0.0090
Ti^{+4}	2625.385	±320.521	0.0146
Al^{+3}	3105.426	±320.252	0.0105
$Fe^{+2}*$	3628.018	±332.137	0.0083
$Mg^{+2} + Ca^{+2}$	3323.320	±318.845	0.0091
K^{+1}	3795.115	±317.215	0.0069
$\frac{Na^{+1}}{Na^{+1}+K^{+1}}$	47.004	±6.333	0.0177

Cations that are combined together in this final equation were selected for combination because they had similar coefficients during preliminary regression analysis. Coefficient $\beta = -3350.650 \pm 320.629$, p value = 0.0090

Table 4 Coefficients for $\ln K_0$ equation

i	θ_i value	Standard error	p value
Si^{+4}	114.098	±32.444	0.0390
$Ti^{+4} + Al^{+3}$	92.263	±32.749	0.0669
$Fe^{+2}* + Ca^{+2} + Na^{+1}$	122.644	±32.578	0.0317
Mg^{+2}	111.549	±32.651	0.0420
K^{+1}	138.855	±34.092	0.0267
$\frac{Na^{+1}}{Na^{+1}+K^{+1}}$	2.239	±0.640	0.0396

Cations that are combined together in this final equation were selected for combination because they had similar coefficients during preliminary regression analysis. Coefficient $\psi = -128.365 \pm 32.578$, p value = 0.0291

$$\ln K_0 = \psi + \sum \left(\theta_i \times D_i\right) \tag{7}$$

where D_i indicates the cation fraction of element i and α_i, β_i, θ, and ψ are coefficients determined from the multiple linear regressions. Values for the coefficients are listed in Tables 3–4. Values of $\ln K_0$ using Eq. 7 require pressure in bars for calculations; if units of MPa are desired, subtract $\ln(0.1)$ from the result of Eq. 7. The values of $\Delta V_r^{0,m}$ and $\ln K_0$ produced by Eqs. 6 and 7 are within ~ 3% and ~ 0.5%, respectively, of the values determined from the experimental data for each of the 10 calibration compositions (Table 2). This analysis suggests that the general model is robust and very accurately predicts CO_2 solubility in these 10 compositions.

Using the general thermodynamic model for CO_2 solubility in mafic magmas

The general model for CO_2 is well-calibrated for magmas that contain 44 wt% to 53 wt% SiO_2 and 2 wt% to 9 wt% total alkalis ($Na_2O + K_2O$) at pressures ranging from ~ 50 MPa to 700 MPa. Here we summarize the general procedure for application of the model to calculate the CO_2 solubility for any mafic magma composition. Calculators are available in the supplementary material (an excel spreadsheet and two Python3 scripts).

We first describe how to use the CO_2 model for a basic system: mafic magma in equilibrium with a pure CO_2 fluid. To begin, calculate the cation fractions for the composition of interest and use Eqs. 6–7 to compute the thermodynamic parameters $\Delta V_r^{0,m}$ and K_0. Next, calculate K (P, T) from Eq. 2; recall that P must be in units of bars, unless the calculated value of K_0 is converted to alternate pressure units. P_0 is 1000 bars and T is 1200 °C (convert T to Kelvin for calculations since gas constant R is present). Finally, use Eqs. 3–5 to transform K (P, T) to wt% CO_2. Note that $f_{CO_2}(P, T)$ in Eq. 3 must be in the same pressure units as P and calculated using the modified Redlich–Kwong equation of state (Holloway 1977, 1981, 1987) with the Saxena and Fei (1987) high-pressure correction as detailed in the appendix of Holloway and Blank (1994). Use of a different equation of state would require recalibration of the thermodynamic parameters. In Eq. 5, the value of FW_{one} should be 36.594 g mol^{-1}, since this constant value was used to determine the thermodynamic parameters for this model.

For mixed-fluid (H_2O–CO_2) compositions, the pressure and fugacity terms in Eqs. 2 and 3, respectively, must be determined based on the proportion of CO_2 in the fluid. To determine the fugacity of CO_2 in a mixed-fluid magma, calculate the pure CO_2 fugacity at the total pressure of the system and then multiply the pure fugacity by the fluid composition $\left(1 - X^f_{H_2O}\right)$. The partial pressure of CO_2 can then be determined from this value of CO_2 fugacity using the equation of state (modified Redlich–Kwong with high pressure correction).

H_2O solubility in mafic magmas

Previous studies have suggested that H_2O is relatively insensitive to melt composition (Moore et al. 1998; Lesne et al. 2011a; Iacono-Marziano et al. 2012). Partly for this reason, the Allison et al. (2019) experiments were not designed to assess H_2O solubility, and those experiments did not show separate trends in H_2O solubility according to composition. To explore the effect of composition on H_2O solubility, we compiled experimental data for 22 mafic magma compositions (anhydrous $SiO_2 < 56$ wt%) with a wide variety of major element compositions (Fig. 4a and supplementary material Table S4) from 14 studies (Cocheo 1994; Dixon et al. 1995; Moore et al. 1995, 1998; Ohlhorst et al. 2001; Berndt et al. 2002; Botcharnikov et al. 2005; Di Matteo et al. 2006; Shishkina et al. 2010, 2014; Lesne et al. 2011a; Vetere et al. 2011, 2014; Iacono-Marziano et al. 2012). The experimental data from these studies is included in the supplementary material (Table S5).

We first examine this data compilation for possible compositional controls on H_2O solubility. We compare the H_2O contents of the experiments with H_2O fugacity, calculated using the modified Redlich–Kwong equation of state (Holloway 1977, 1981, 1987) with the Saxena and Fei (1987) high-pressure correction as detailed in the appendix of Holloway and Blank (1994). For mixed-fluid experiments, we calculate the pure H_2O fugacity at the total pressure of the experiment and then multiply it by the experiment fluid composition ($X^f_{H_2O}$) to determine H_2O fugacity. For clarity the data are separated into two groups: roughly half of the experiments, those with compositions falling within the grey region of Fig. 4a, are shown in Fig. 4b, while the remaining experiments are shown in an identical plot in Fig. 4c. In Fig. 4b, c, we also plot the power-law fit for the Etna composition from Lesne et al. (2011a) for comparison:

$$f_{H_2O}^{1200\,^\circ C} = 104.98 \times \text{wt\% } H_2O^{1.83} \quad (8)$$

in which fugacity is in units of bars.

Overall, the H_2O solubility data (Fig. 4b, c) do not show any clear relationship to composition, and most of the experiments closely follow the Lesne et al. (2011a) power-law fit for Etna (Eq. 8). Note that the experimental data (Fig. 4b, c) is quite limited above ~ 5 wt% H_2O, which likely reflects the difficulty in quenching hydrous glasses. This data compilation lends further support to the conclusion of previous studies (e.g., Moore et al. 1998; Lesne et al. 2011a; Iacono-Marziano et al. 2012) that H_2O solubility in mafic magmas is not strongly affected by melt composition. If there is an effect, it cannot be resolved over the broad compositional range of the current experimental literature, but it merits future careful investigation.

There exist several H_2O solubility models calibrated specifically for alkali-rich mafic magmas (e.g., Iacono-Marziano et al. 2012; Shishkina et al. 2014), and we next evaluate how these models perform for this compilation of data. We plot the difference between the experimental data and the model-calculated H_2O solubility in Fig. 4d, e. The average difference between measured H_2O and calculations of H_2O content using the Lesne et al. (2011a) power-law fit for Etna for all experiments in this compilation is 0.35 wt% (median: 0.25 wt%), with a maximum difference of 1.68 wt%. Using the Iacono-Marziano et al. (2012) model, however, the average difference

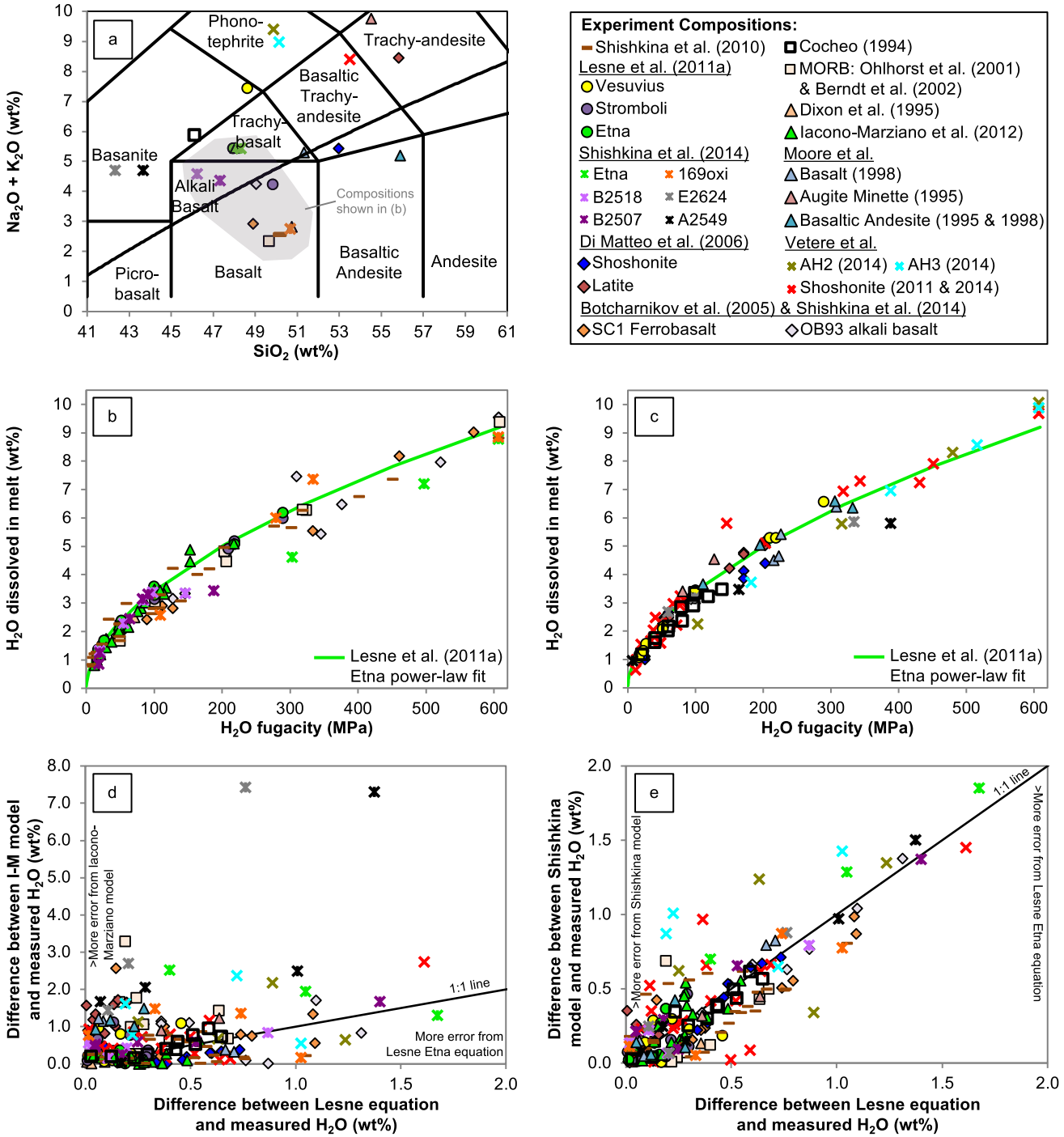

Fig. 4 H_2O solubility experiments compared with models for mafic magmas. **a** Total alkali and silica compositions of experiments. **b** Experiments for compositions in the grey region of (**a**) compared with the Lesne et al. (2011a) power-law equation for the Etna composition. **c** Same as (**b**) except the experiments shown are for the compositions beyond the grey region of (**a**). **d**, **e** Evaluation of the accuracy of different models for H_2O solubility, shown as differences between the experimental data and predictions from models. Results from the Lesne et al. (2011a) power-law equation for Etna are compared with the Iacono-Marziano et al. (2012) model in (**d**) and the Shishkina et al. (2014) model in (**e**)

is 0.70 wt% (median: 0.41 wt%), with two notable outliers at 7.43 and 7.30 wt% (Fig. 4d). We note that these two outliers are experiments published in 2014 (after the Iacono-Marziano et al. 2012 model), and the maximum difference between this model and measured H_2O for all other experiments in this compilation is 3.30 wt%. For the Shishkina et al. (2014) model

(Fig. 4e), the average and median differences between the experiments and this model are identical to those for the Lesne et al. (2011a) Etna fit, with a slightly higher maximum difference of 1.85 wt%. However, due to the polynomial formulation of the empirical Shishkina et al. (2014) model, it yields non-zero values for H_2O solubility at 0 MPa that depend solely on Na + K cation fraction. For the compositions in Fig. 4, the Shishkina et al. (2014) model calculates concentrations of H_2O at 0 MPa ranging from 0.97 to 1.08 wt%. Previous experimental work suggests that H_2O solubility in mafic magmas (i.e., tholeiite) near 0 MPa is much lower than 1 wt% (~0.1 wt% at 1 atm; Baker and Grove 1985).

It is apparent that models relating H_2O solubility in mafic magmas to compositional components generally show more disagreement with the experimental data than calculations using a single empirical fit (Fig. 4d, e). Our data compilation shows an uneven distribution of experiments by pressure (more experiments at lower pressures) as well as differences in the number of experiments available for each composition. For these reasons, we do not calibrate a new empirical equation from the data compilation and instead use the Lesne et al. (2011a) power-law fit for Etna (Eq. 8) to calculate H_2O solubility in mafic magmas. The calculators available in the supplementary material use Eq. 8 for the H_2O model (in conjunction with the thermodynamic CO_2 model) for all mixed-fluid determinations.

To use Eq. 8 for H_2O solubility in conjunction with the general thermodynamic model for CO_2 solubility to determine volatile solubilities for mixed-fluid (H_2O–CO_2) magmas, we determine partial pressures of H_2O and CO_2 using the equation of state and fluid composition of the system. To determine the fugacity of H_2O in a mixed-fluid magma, we calculate the pure H_2O fugacity at the total pressure of the system and then multiply the pure fugacity by the fluid composition $\left(X^f_{H_2O}\right)$. The partial pressure of H_2O can then be determined from this value of H_2O fugacity using the equation of state (modified Redlich–Kwong with high pressure correction). For example, a magma at 500 MPa and 1200 °C with a pure fluid composition (i.e., 100% H_2O or CO_2) would have a pure H_2O fugacity of 607 MPa $\left(X^f_{H_2O} = 1\right)$ or a pure CO_2 fugacity of 1610 MPa $\left(X^f_{H_2O} = 0\right)$. At these same *P*–*T* conditions, a mixed-fluid experiment with fluid composition of 0.2 $X^f_{H_2O}$ will have H_2O fugacity of 121 MPa, which corresponds to a partial pressure of 122 MPa for H_2O. The CO_2 fugacity for this fluid composition is 1288 MPa, corresponding to a partial pressure of 451 MPa for CO_2.

Testing the MafiCH model for H_2O–CO_2 solubility in mafic magmas

A robust general model should be capable of predicting solubility relationships for a variety of mafic compositions for which volatile solubility has not been experimentally determined. To test the validity of the MafiCH model for unstudied compositions, we compare the model calculations with recent experimental data at 1200–1250 °C between 50 and 500 MPa from Fanara et al. (2015) and Schanofski et al. (2019). The magma compositions are a "trachybasalt" with 49 wt% SiO_2 and 4.4 wt% $Na_2O + K_2O$ from Fanara et al. (2015) and from Schanofski et al. (2019), a leucitite with 44.5 wt% SiO_2 and 12 wt% $Na_2O + K_2O$ and phonolite with 56 wt% SiO_2 and 15.4 wt% $Na_2O + K_2O$. Note that Fanara et al. (2015) refer to this composition as "trachybasalt" because it was synthesized to reproduce a natural trachybasalt from the Campanian Ignimbrite, but the starting glass composition is alkali basalt. The "trachybasalt" magma from Fanara et al. (2015) is within the calibrated compositional range of the MafiCH model (Fig. 5). The leucitite magma from Schanofski et al. (2019) has higher *K* content than the calibration compositions but is otherwise within the calibrated range. The phonolite composition from Schanofski et al. (2019) is beyond the calibrated compositional range of the CO_2 model (Fig. 5) for all elements except Ti and Na. We

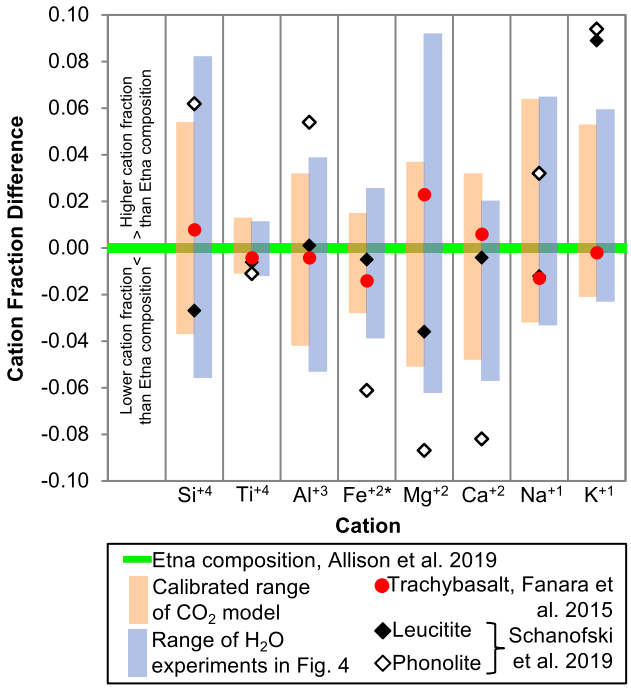

Fig. 5 Compositions from Fanara et al. (2015) and Schanofski et al. (2019) compared with the compositional range of experiments used to calibrate H_2O and CO_2 models. Cation fractions are plotted relative to the Etna composition from Allison et al. (2019)

don't specifically intend for MafiCH to be used to constrain volatile solubility in polymerized melts such as a phonolite, but we test this composition to examine the performance of the model when extrapolated beyond its calibrated range. Results from the comparison between the MafiCH model and experiments from these three compositions are shown in Fig. 6.

Of note, both Fanara et al. (2015) and Schanofski et al. (2019) determine fluid compositions using the mass-loss method, though neither study provided error estimates for the $X^f_{H_2O}$ values. In the mass-loss method, the experiment capsule is first weighed, and then frozen in liquid nitrogen prior to and during puncture. The capsule is next allowed to warm to room temperature to release the CO_2 fluid and re-weighed. Finally, the capsule is stored in a drying oven to release the H_2O fluid and weighed again. There are a few sources of uncertainty involved in mass-loss fluid determinations that were mentioned in these studies, including balance error, incomplete fluid separation, and mixed-fluid bubbles bursting during oven heating. These sources of uncertainty are discussed in further detail in the supplementary material and Figs. S1, S2. Overall, larger uncertainties in $X^f_{H_2O}$ are expected for experiments that include small masses (< 1 mg) of one or both fluids. Additionally, uncertainty in $X^f_{H_2O}$ propagates to greater uncertainty in fugacity at higher pressure. So, while we do not show error bars for fugacities in Fig. 6, we note that based on the calculations shown in the supplementary material, uncertainty in fluid composition can produce fugacity errors of hundreds of MPa, particularly at high fugacities.

The MafiCH model shows strong agreement with the experimental data from the "trachybasalt" composition from Fanara et al. (2015) (Fig. 6a, b). The vast majority of these experiments define trends that align closely with both the CO_2 and H_2O models. The experiment with the highest CO_2 fugacity appears to notably deviate from the CO_2 model, but this discrepancy could perhaps be partly explained by errors in the fluid measurement $\left(X^f_{H_2O}\right)$. This particular experiment contained ~ 10 mg of CO_2 in the fluid and only 1 mg of H_2O.

The MafiCH model shows excellent agreement with the experimental data from the leucitite composition (Fig. 6c, d). The CO_2 model in particular is remarkably well suited to this experimental data. All but two experiments are within 500 ppm CO_2 of the model calculations, and most overlap with the model when analytical error is accounted for. The H_2O data is generally offset to slightly higher H_2O (average: 0.34 wt%) compared with the model, but many experiments, especially those with < 5 wt% H_2O, do agree with the model within error.

The phonolite experiments illustrate the performance of the CO_2 model in MafiCH beyond its calibrated range as well as its limitations. Roughly one third of the experiments for the more evolved phonolite composition show strong agreement with the CO_2 model, but the others diverge to lower CO_2 contents than predicted by the model (Fig. 6e). The experiments that follow the modeled solubilities all exhibit fluid compositions of $X^f_{H_2O} > 0.4$. At drier compositions, however, the model and experiments deviate significantly (up to 1100 ppm difference), with the experiments showing lower CO_2 solubility than what is calculated by the model. Schanofski et al. (2019) discuss this difference in CO_2 solubility at dry vs. wet conditions, and attribute it to the effect of H_2O on the polymerization of the melt. At high H_2O contents and $X^f_{H_2O}$, H_2O breaks up tetrahedra in the melt structure, and thus more CO_2 can be incorporated into the melt structure (e.g., Mysen 1976). These results suggest that the CO_2 model works well for relatively depolymerized melts (i.e., mafic magmas and hydrous intermediate magmas with CO_2 stored as CO_3), but does not accurately constrain solubility for polymerized melts beyond its calibrated range.

For H_2O, the phonolite experiments generally follow the MafiCH model, with some variability (Fig. 6f). Note that some of the phonolite experiments were determined by Schanofski et al. (2019) to have large errors in their fluid compositions as a result of mixed-fluid bubbles bursting during oven drying, and these experiments are marked with an x in Fig. 6e, f. Excluding the experiments with large fluid composition errors, the average difference between the H_2O model and phonolite experiments is 0.34 wt%, identical to that of the leucitite experiments. In the phonolite experiments, however, the deviation from the model differs based on the amount of H_2O in the experiments. At low H_2O contents (< 3 wt%), the model predicts slightly higher H_2O than the experiments, while at higher H_2O (> 5 wt%) the model predicts slightly lower H_2O. The experiments and H_2O model show strong agreement between 3 and 6 wt%.

Overall, these tests suggest that the MafiCH model is accurate within its calibrated range, and in some cases (i.e., depolymerized melts) may apply beyond this compositional range. We recommend comparing the cation fractions of the composition of interest to the calibrated ranges shown in Fig. 5 to determine whether the MafiCH model will be useful for a specific volcanic system.

Implications

Volcanic plumbing systems: saturation pressures from previously published solubility models

Melt inclusion volatile contents are commonly used to interpret the depth of melt inclusion formation and crystal residence and therefore magma storage and structure of the volcanic plumbing system (e.g., Lowenstern 1995). Volatile

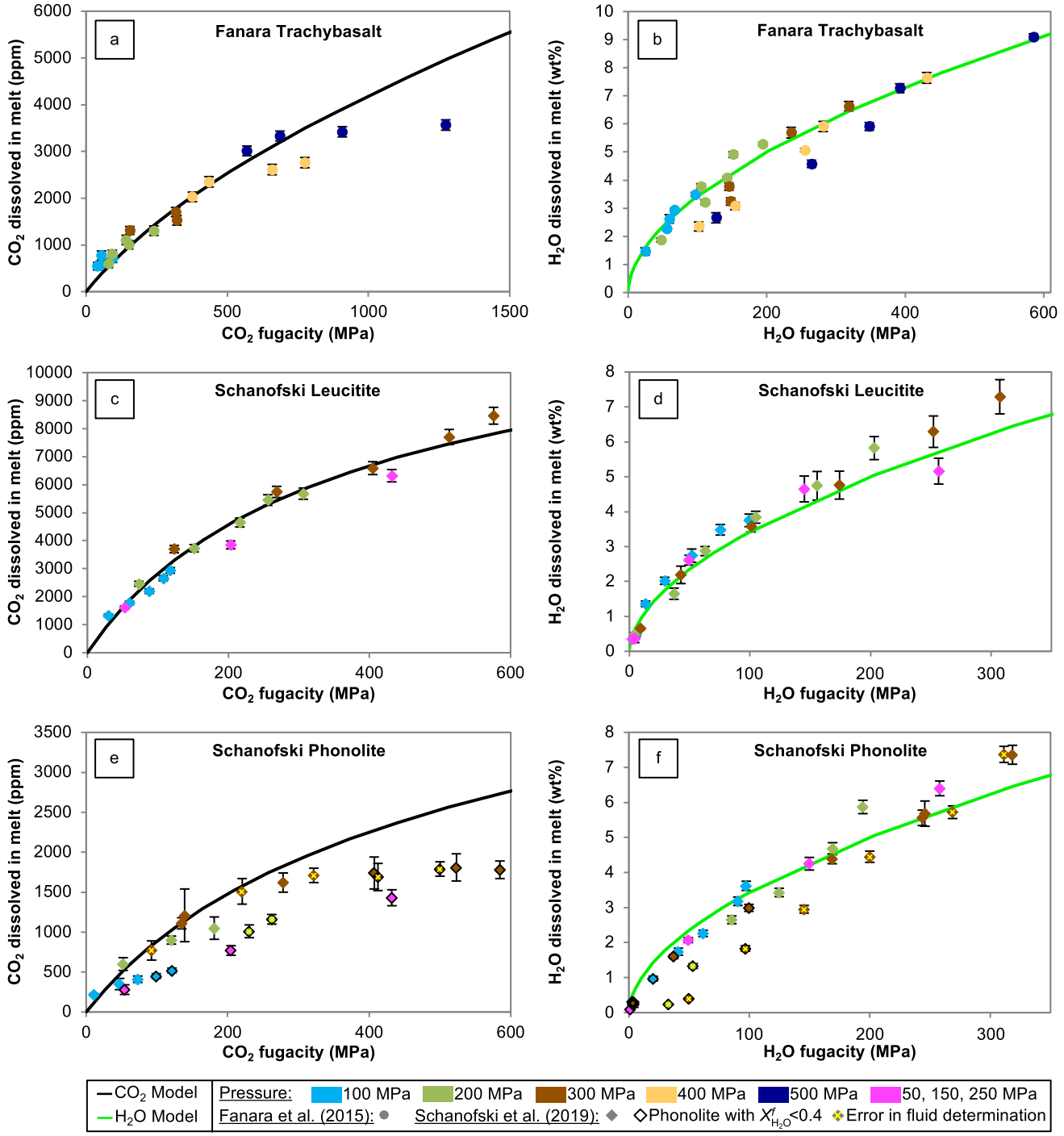

Fig. 6 Comparison between the model presented here (curves) and experiments (symbols) from Fanara et al. (2015) and Schanofski et al. (2019). Colors of symbols correspond to the total pressure of the experiment. Fugacities of the experiments were calculated using the equations of state for H_2O and CO_2 used in Allison et al. (2019). Panels in the left column show CO_2 data and panels in the right column show H_2O data. Top row shows the trachybasalt composition from Fanara et al. (2015); middle row shows the leucitite composition from Schanofski et al. (2019); bottom row shows the phonolite composition from Schanofski et al. (2019). Error bars correspond to the values given in Fanara et al. (2015) and Schanofski et al. (2019). No error bars are shown for fugacity as these studies did not provide error estimates for fluid compositions, aside from noting specific experiments of the Phonolite composition from Schanofski et al. (2019) with a large error in the determination of $X^f_{H_2O}$ (identified here by symbols containing an x). Phonolite experiments with $X^f_{H_2O}<0.4$ are shown with outlined symbols to indicate experiments with the most polymerized melt structures

solubility models are used to calculate the pressure at which the melt inclusion volatiles are saturated in the magma to provide minimum depth estimates. Different solubility models will yield different melt inclusion entrapment pressures (e.g., Fig. 1), which will affect interpretation of the volcanic system.

To compare how different solubility models affect the interpretation of volcanic data, we determine saturation pressures at 1200 °C for hypothetical melt inclusion volatile compositions. We chose conditions for which the new MafiCH model is particularly well calibrated to serve as a reference. In particular, the hypothetical melt inclusion volatile composition is relatively CO_2-rich to take advantage of the 400–600 MPa experiments from Allison et al. (2019) that form the core data set for model calibration. In the supplementary material, we show the results of this same test for two additional melt inclusion volatile compositions (Figs. S3, S4). We focus on only one volatile composition here, as the overall trends in calculated saturation pressures are largely the same for these three different melt inclusion volatile compositions.

We show saturation pressures calculated for a melt inclusion with 2.5 wt% H_2O and 4000 ppm CO_2 in Fig. 7. The saturation pressures are plotted for each of the 10 calibration compositions for the MafiCH CO_2 model according to the wt% total alkali content of the magma for ease of visualization. The major element compositions of these magmas are included in the supplementary material (Table S2). For models that require Fe speciation, we convert from total Fe assuming an oxidation state of NNO + 1 using Kilinc et al. (1983).

First, we discuss the results from the oldest and newest models being tested in comparison to the new MafiCH model (Fig. 7a, b): VolatileCalc (Newman and Lowenstern 2002) and MagmaSat (Ghiorso and Gualda 2015). VolatileCalc is unable to calculate saturation pressures for three compositions (basalt N72, basaltic andesite SFVF, and phonotephrite AH3) as they have > 49 wt% SiO_2. For the SiO_2 input for VolatileCalc calculations, we use the SiO_2 value that results from normalizing to 100% anhydrous after conversion of total Fe to FeO and Fe_2O_3. There is a significant misfit between VolatileCalc and the new MafiCH model for the Vesuvius (~ 280 MPa) and Stromboli (~ 190 MPa) compositions, and lower, but still notable misfit for the leucitite (~ 115 MPa) and Etna (~ 90 MPa) compositions. The results from VolatileCalc are largely similar to the new MafiCH model for the remaining three compositions (Sunset Crater, Erebus, and the basanite; < 30 MPa difference). For the most volatile-rich melt inclusion composition (4.5 wt% H_2O and 4000 ppm CO_2; see supplementary material Fig. S4), increasing divergence between VolatileCalc and the new MafiCH model occurs, and noticeable misfits appear for all compositions. The VolatileCalc model is not intended for use at pressures above 500 MPa, and these results illustrate that it is not well calibrated at these high pressures as it calculates saturation pressures that are much higher than what are indicated by the latest experimental data. MagmaSat agrees very closely with the new MafiCH model for these three hypothetical melt inclusion compositions for the magmas with > 5.5 wt% alkalis. There is some disagreement, however, between MagmaSat and MafiCH for the compositions with lower total alkali contents, particularly the basalt (N72) and basaltic andesite (SFVF) magmas.

Next, we examine the two other comprehensive models (Fig. 7c, d): Papale et al. (2006) and Duan (2014). The Papale et al. (2006) model calculates very similar saturation pressures for magmas across this entire compositional range, with only ~ 132 MPa difference between the lowest and highest saturation pressures (Fig. 7c). The range of saturation pressures predicted by MafiCH is nearly 3× wider (371 MPa difference between the lowest and highest pressures) than the Papale et al. (2006) calculations. The Papale et al. (2006) model shows strong agreement with the new MafiCH model for the Sunset Crater alkali basalt composition and moderate agreement (~ 50–60 MPa difference) for SFVF, Etna, Stromboli, and Erebus. For the remaining compositions, the Papale et al. (2006) model shows poor agreement with the MafiCH model (> 100 MPa difference), with particular misfits for the AH3 phonotephrite (~ 285 MPa difference) and leucitite (~ 205 MPa difference). The Duan (2014) model generally calculates higher saturation pressures for each composition compared with the new MafiCH model, though it calculates lower saturation pressures for the Vesuvius composition. The Duan (2014) model agrees with the new MafiCH model for two very different compositions: the Stromboli alkali basalt and Erebus phonotephrite. The Duan (2014) model also shows moderate agreement with the new MafiCH model for the Vesuvius composition (~ 55 MPa difference), but poor agreement (> 100 MPa difference) for the remaining seven compositions. Another interesting note is that both the Duan (2014) and Papale et al. (2006) models calculate nearly identical saturation pressures for the Erebus and AH3 compositions, which have similarly high total alkali contents but significant compositional differences in other elements. Experimental data and the new MafiCH model show drastically different CO_2 solubilities for the Erebus and AH3 magmas.

Finally, we compare pressures calculated using the two models that are specific to mafic magmas (Fig. 7e, f): Iacono-Marziano et al. (2012) and Shishkina et al. (2014). The Shishkina et al. (2014) model consistently calculates higher pressures than the new MafiCH model, while the Iacono-Marziano et al. (2012) model consistently calculates lower pressures. There are noticeable

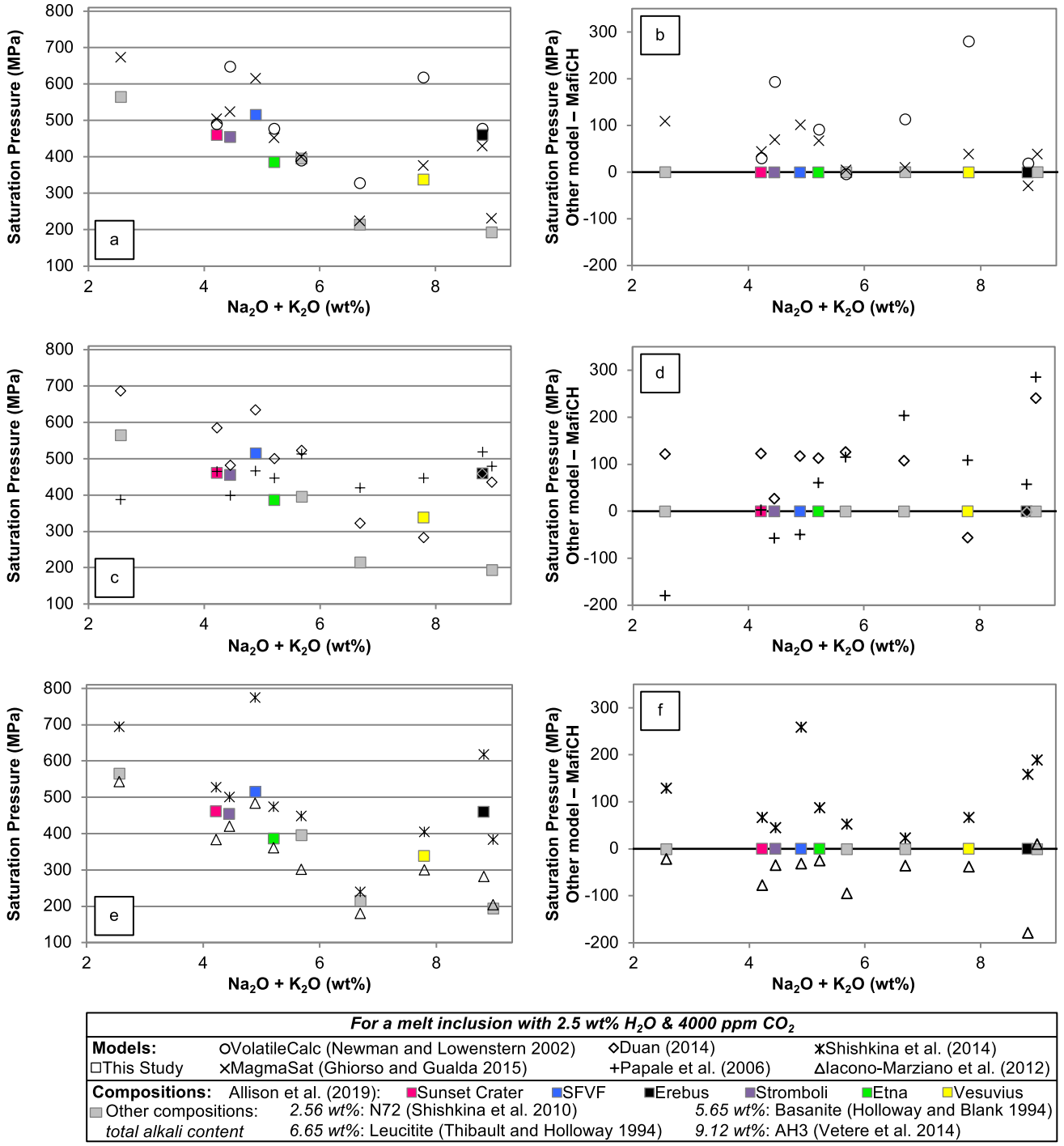

Fig. 7 Saturation pressures calculated from six previously published volatile solubility models compared with the new MafiCH model for a theoretical melt inclusion composition at 1200 °C with 2.5 wt% H_2O and 4000 ppm CO_2. Saturation pressures are shown in panels in the left column and the differences in saturation pressure from the MafiCH model are shown in panels in the right column. The MafiCH model (squares) is compared with two previously published models in each row: (top) VolatileCalc (Newman and Lowenstern 2002) and MagmaSat (Ghiorso and Gualda 2015); (middle) Duan (2014) and Papale et al. (2006); (bottom) Shishkina et al. (2014) and Iacono-Marziano et al. (2012). Results are plotted according to total alkali content of the magma compositions

misfits between the Shishkina et al. (2014) model and the new MafiCH model, specifically for the basaltic andesite (SFVF; ~ 260 MPa difference), basalt (N72; ~ 130 MPa difference), as well as the compositions with the highest alkali contents, AH3 (~ 190 MPa difference) and Erebus (~ 160 MPa difference). The Iacono-Marziano et al. (2012)

model shows strong divergence from the new MafiCH model for the Erebus (~ 180 MPa difference) composition and moderate disagreement for the basanite (~ 95 MPa difference) and Sunset Crater (~ 75 MPa difference) compositions. For the remaining compositions, the pressures from Iacono-Marziano et al. (2012) agree with the MafiCH model within < 50 MPa.

Overall, VolatileCalc (Newman and Lowenstern 2002), Duan (2014), and Shishkina (2014) tend to calculate higher saturation pressures than the new model, while the Iacono-Marziano et al. (2012) model consistently yields lower saturation pressures. The Papale et al. (2006) model returns very similar saturation pressures for these 10 mafic compositions of variable alkali contents, suggesting that it is not well suited to distinguish solubility differences in this compositional range. Saturation pressures in Fig. 7 calculated using the Iacono-Marziano et al. (2012) and MagmaSat (Ghiorso and Gualda 2015) models have the smallest average difference (~ 50 MPa) from the MafiCH model for these 10 compositions. However, we note that we chose to focus on relatively hydrous volatile compositions for this test to avoid bias in saturation pressures as a result of variable isobar shapes at low H_2O contents (see Fig. 1). The Iacono-Marziano et al. (2012) and MagmaSat (Ghiorso and Gualda 2015) models in particular show a strong decrease in CO_2 solubility at low H_2O contents, and would therefore show larger deviations from MafiCH at relatively anhydrous compositions. The behavior of CO_2 solubility at low H_2O is poorly understood at present, so the different trends shown by models at H_2O-poor fluid compositions are relatively unconstrained.

The degree of consensus between models also varies based on the overall magma composition. Pressures calculated for the Sunset Crater alkali basalt show the best agreement for all models; in Fig. 7, the average difference between each model and the MafiCH model is just ~ 55 MPa for Sunset Crater. The models show significant disagreement (> 100 MPa average difference from MafiCH in Fig. 7) for the highest silica composition (SFVF basaltic andesite), as well as the compositions at the extremes of total alkali contents in this range (< 3 wt% and > 7 wt%). These significant disagreements may indicate that these compositional ranges are at or beyond the calibrated limits of the previous models. Some of these differences are likely due to the fact that some models attribute most of the compositional dependence of CO_2 solubility in mafic magmas to total alkali contents rather than the full multicomponent magma composition. The Erebus magma, for example, is one of the compositions that show a wide range of saturation pressures predicted by the different models. Erebus has high total alkali contents, corresponding to high CO_2 solubility in some models, but it also has the lowest Ca cation fraction and highest Al cation fraction in our calibration dataset, resulting in lower CO_2 solubility in other models.

One final interesting observation from Fig. 7 is the relative solubility differences between the magmas. In the compositions assessed in Fig. 7, saturation pressures generally decrease (i.e., volatile solubility increases) with increasing total alkali content, with the exception of magmas with higher silica contents (i.e., the SFVF composition) and very high total alkali contents (> 6 wt%). With the exception of VolatileCalc (Newman and Lowenstern 2002) and the Papale et al. (2006) model, the newer models generally replicate these same overall trends of volatile solubility with total alkali content. This may suggest that models have now identified the major elemental impacts on volatile solubility in mafic magmas, even though the models do vary in their overall calibration. If that is the case, future work to refine the models should focus on compositions for which the recent models do not converge (i.e., basaltic andesites and magmas with high total alkali contents).

Relative influence of compositional components on CO_2 solubility (what affects CO_2 solubility?)

Previous models specific to mafic magmas have correlated solubility relationships with compositional parameters that range from single elements to multicomponent calculations. For example, VolatileCalc (Newman and Lowenstern 2002) uses the SiO_2 content (wt%) as a proxy for the compositional parameter Π from Dixon (1997). Iacono-Marziano et al. (2012) and Shishkina et al. (2014) use more complex compositional parameters (NBO/O and Π*, respectively) to correlate with CO_2 solubility. In Fig. 8 we compare the calculated CO_2 solubility from MafiCH at 500 MPa and 1200 °C for the 10 calibration compositions compared with these compositional parameters.

Figure 8a shows essentially no correlation between CO_2 solubility and SiO_2 content (wt%). This is unsurprising, because the SiO_2 parameterization incorporated into VolatileCalc (Newman and Lowenstern 2002) was based on suite of samples from a single submarine location and not intended for broad application. The NBO/O parameter used by the Iacono-Marziano et al. (2012) model also shows very little correlation with CO_2 solubility as determined by MafiCH (Fig. 8b). In fact, three of these compositions have nearly identical values of NBO/O but very different CO_2 solubilities (~ 6000–13,000 ppm CO_2 at 500 MPa and 1200 °C). The Π* parameter used by Shishkina et al. (2014) does appear to capture much of the variability in CO_2 solubility by these magmas, although the relationship between Π* and CO_2 solubility is non-linear (Fig. 8c). Recent work by Mangan et al. (2021) suggested that CO_2 solubility may

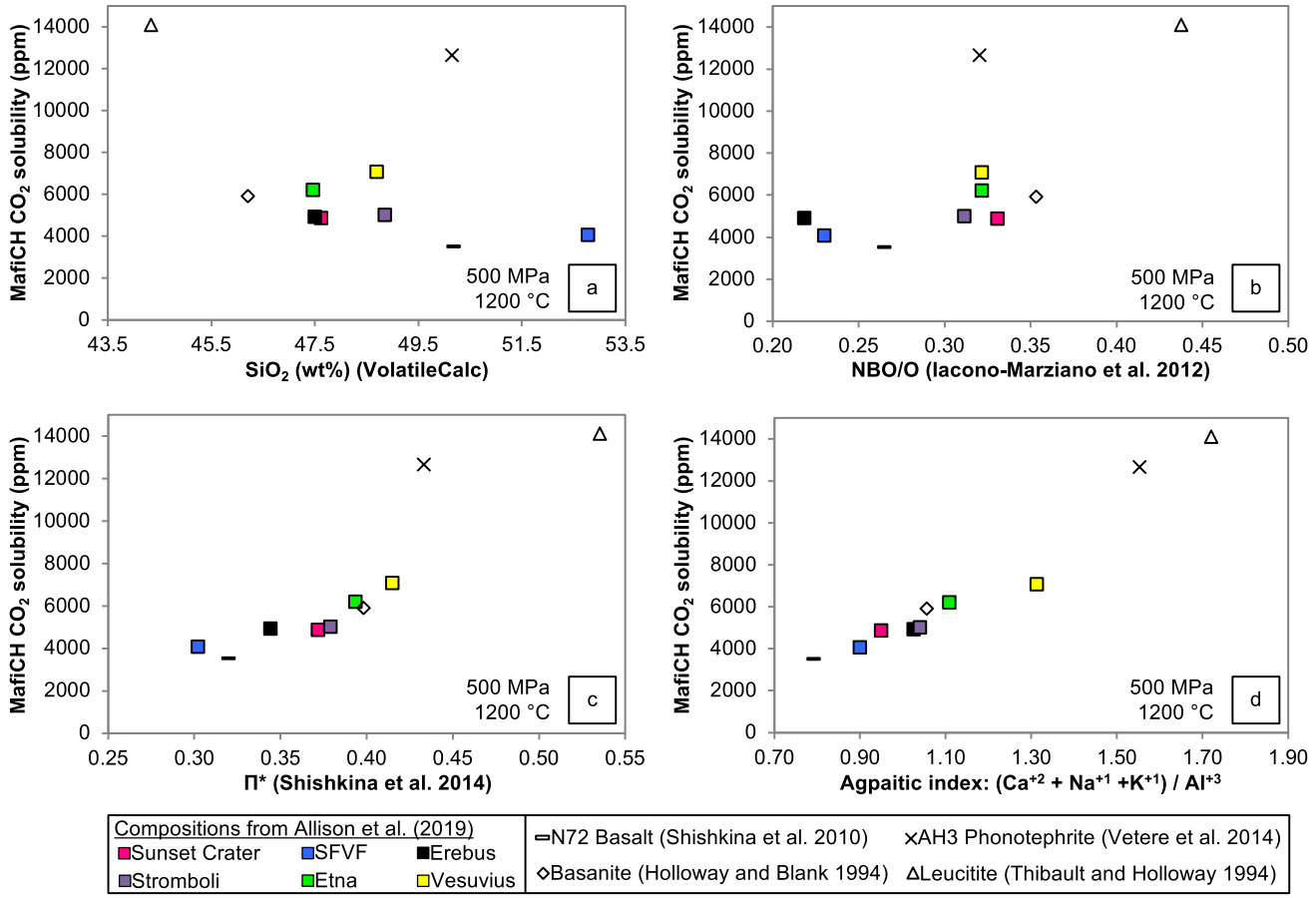

Fig. 8 Comparison of CO_2 solubility at 500 MPa and 1200 °C calculated by the MafiCH model with compositional parameters from other works. CO_2 solubilities are calculated for the 10 calibration compositions in the CO_2 model of MafiCH. The parameters are: **a** SiO_2 content in wt% from VolatileCalc (Newman and Lowenstern 2002), **b** NBO/O from Iacono-Marziano et al. (2012), **c** Π^* from Shishkina et al. (2014), and **d** agpaitic index $(Ca^{+2}+Na^{+1}+K^{1})/Al^{+3}$ as described in Mangan et al. (2021)

be related to the agpaitic index of a magma, defined as $(Ca^{+2}+Na^{+1}+K^{+1})/Al^{+3}$. The MafiCH model supports this conclusion, showing a strong positive correlation between CO_2 solubility and agpaitic index (Fig. 8d). The agpaitic index correlation helps to explain why two compositions with similar total alkali contents (i.e., Erebus and AH3) can have very different CO_2 solubilities.

Because the CO_2 model in MafiCH does provide accurate solubility relationships for a variety of mafic compositions (e.g., Fig. 6a and c), we make an assumption that it can be used to test how small changes in composition impact CO_2 solubility, especially when interpolating between calibrated compositions. While this is a significant assumption, this exercise may provide useful insights about the mechanism of CO_2 dissolution in mafic magmas and changes in volatile solubility during magma evolution or for closely associated magmas, as well as identify priorities for future experimental investigations.

To investigate the influence of compositional components on CO_2 solubility, we determine the expected change in solubility when the abundance of one cation component is varied (Figs. 9, 10). We first calculate the CO_2 solubility at 500 MPa and 1200 °C for a specific composition, represented by the asterisk. We then change just one cation component of this composition in 0.005 increments and renormalize all cations at each step. Then, using the MafiCH model, we recalculate $\ln K_0$ and $\Delta V_r^{0,m}$ and determine the new CO_2 solubility as a result of this change in composition. Note that symbols in grey in Figs. 9, 10 indicate that the calculated cation fraction is beyond the calibrated range of the model.

Figure 9 depicts the influence of sodium, potassium, calcium, and silicon content on CO_2 solubility according to the MafiCH model. We show the results of these tests for the Sunset Crater (Fig. 9a), Erebus (Fig. 9b), and Stromboli (Fig. 9c) magmas because they exhibit nearly identical CO_2 solubilities despite their variable chemical compositions. We also examine the Etna composition (Fig. 9d) as it is fairly similar in composition to the Sunset Crater magma yet has a higher CO_2 solubility. The remaining compositions used

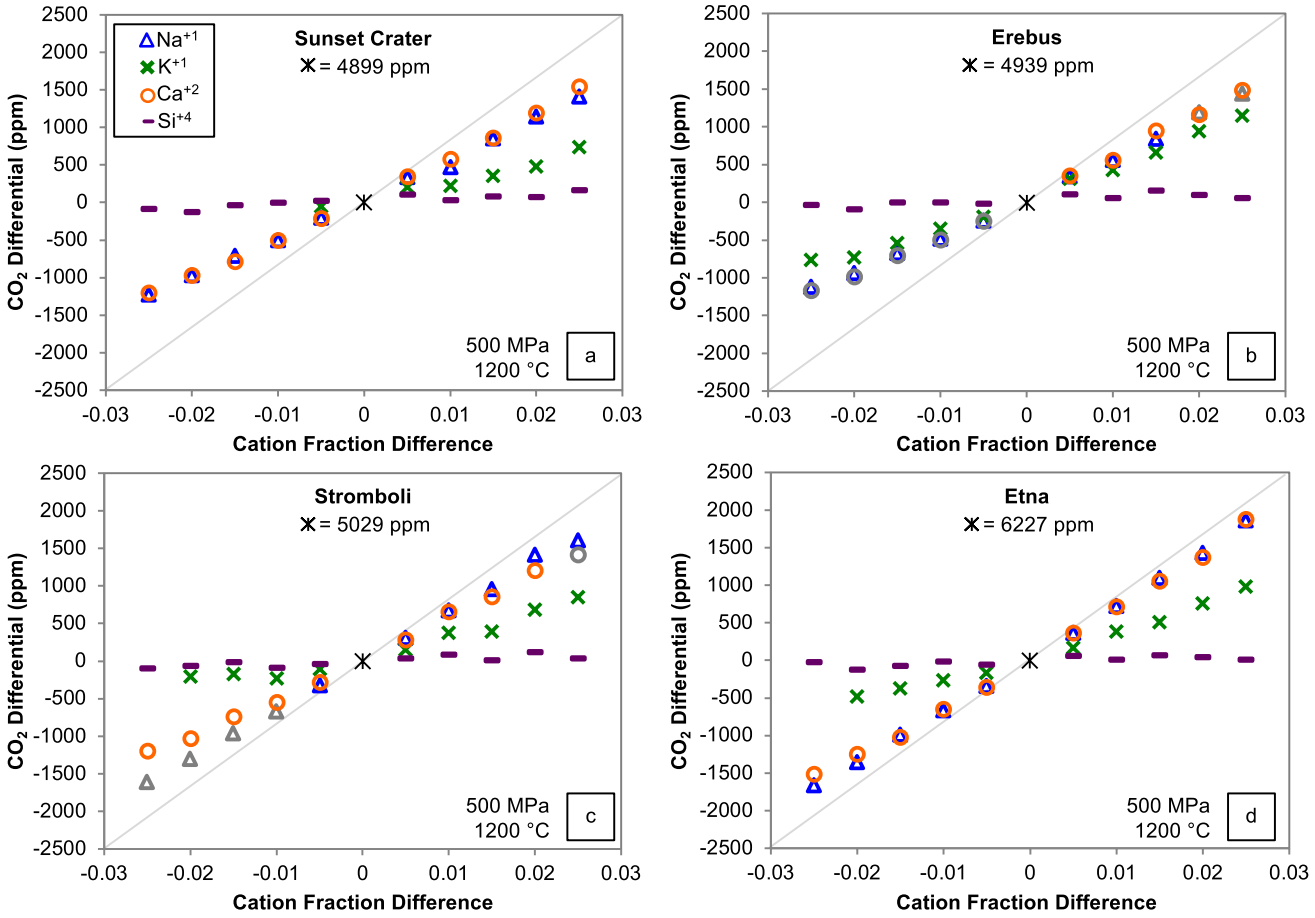

Fig. 9 Predicted influence of Na^{+1}, K^{+1}, Ca^{+2}, and Si^{+4} on CO_2 solubility according to the MafiCH model. CO_2 solubility (dissolved CO_2 content) calculated by the model at 500 MPa and 1200 °C for the **a** Sunset Crater, **b** Erebus, **c** Stromboli, and **d** Etna compositions is shown by the asterisk symbol. Additional symbols show how calculated solubility (at 500 MPa and 1200 °C) changes as one component is varied (single cation fraction in 5% intervals). At each step the modified composition is re-normalized to determine new values of $\ln K_0$ and $\Delta V_r^{0,m}$. Symbols in grey indicate that the calculated cation fraction is beyond the calibrated range of the model. Diagonal lines are drawn to aid in comparisons between panels

to calibrate the CO_2 model display similar overall trends to those in Fig. 9. According to this test, Si^{+4}, which is the sole compositional input (as SiO_2) in the VolatileCalc model (Newman and Lowenstern 2002), has essentially no impact on CO_2 solubility in this compositional range. This is an interesting, but perhaps expected result as SiO_2 content was only used as a proxy for the compositional parameter Π from Dixon (1997) for a specific set of samples. This SiO_2 proxy was not intended to be broadly applied to a wide range of mafic magmas.

The effect of potassium on CO_2 solubility according to the MafiCH model is variable and non-linear. Its effect on CO_2 solubility is low in the Sunset Crater composition (Fig. 9a), slightly stronger for Stromboli (Fig. 9c) and Etna (Fig. 9d), and it has a very strong effect in the Erebus magma, nearly equal to the effect to calcium and sodium (Fig. 9b). However, the impact of potassium on CO_2 solubility appears to be much lower at low K^{+1} contents. For example, in the Stromboli composition (0.023 initial K^{+1}; Fig. 9c), the addition of potassium has a positive effect on CO_2 solubility, but there is essentially no change in solubility if potassium is subtracted. In the Erebus magma (0.033 initial K^{+1}; Fig. 9b), however, CO_2 solubility does show a notable decrease as potassium content is decreased.

Calcium and sodium exhibit the strongest positive effects on CO_2 solubility based on the results shown in Fig. 9, but the effects vary across these four compositions. The magnitude of the solubility increase due to increased calcium or sodium is smaller for Sunset Crater (Fig. 9a) and Erebus (Fig. 9b) compared to Stromboli (Fig. 9c) and Etna (Fig. 9d). Furthermore, in the Sunset Crater and Erebus compositions, addition of calcium has a slightly stronger effect on CO_2 solubility than the addition of sodium, whereas for the Stromboli composition (Fig. 9c), addition of sodium has the larger effect. In the Etna composition (Fig. 9d), addition of

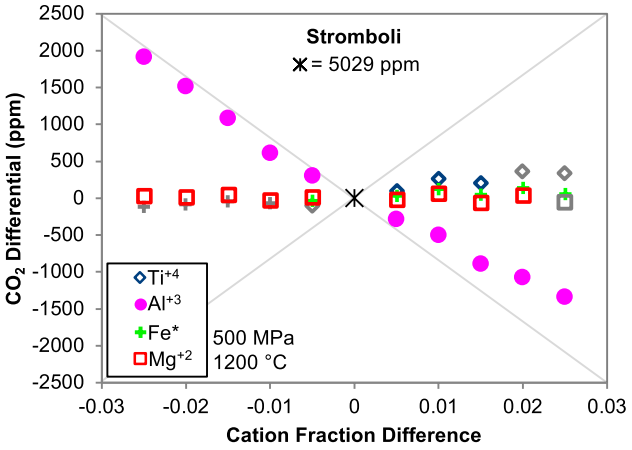

Fig. 10 Predicted influence of Ti^{+4}, Al^{+3}, Fe*, and Mg^{+2} on CO_2 solubility according to the MafiCH model. CO_2 solubility (dissolved CO_2 content) calculated by the model at 500 MPa and 1200 °C for the Stromboli composition is shown by the asterisk symbol. Additional symbols show how calculated solubility (at 500 MPa and 1200 °C) changes as one component is varied (single cation fraction in 5% intervals). At each step the modified composition is re-normalized to determine new values of $\ln K_0$ and $\Delta V_r^{0,m}$. Symbols in grey indicate that the calculated cation fraction is beyond the calibrated range of the model. Diagonal lines are included for visual reference and easy comparison to Fig. 9

sodium has a nearly equal impact on CO_2 solubility as the addition of calcium.

We also examine the influence of titanium, aluminum, iron, and magnesium content on CO_2 solubility according to the MafiCH model in Fig. 10. Figure 10 was constructed following the same method that was used for Fig. 9. For these elements, the overall trends are the same for all 10 magma compositions used to calibrate the CO_2 model, and so we focus only on the results for the Stromboli composition. Aluminum has a very strong negative effect on solubility, nearly as strong as the positive effect of calcium and sodium. This is likely because in order for Al^{+3} to form a tetrahedron with oxygen, it requires an additional cation, like K^{+1} or Na^{+1} to charge balance the tetrahedron. So not only does aluminum serve to polymerize the melt by forming a tetrahedron, but it also prevents one of these alkali cations from bonding with carbonate, leading to a very strong effect on CO_2 solubility. The remaining elements in Fig. 10 appear to have very little effect on CO_2 solubility in these compositions. Overall, this analysis (Fig. 9, 10) illustrates the complexity of CO_2 solubility. The influence of each individual component appears to depend upon the abundance of other components. Also, this result demonstrates that it is necessary to use the full multi-component melt composition to build well-calibrated solubility models.

Conclusions

We developed a general thermodynamic model for CO_2 solubility in mafic magmas across a wide range of total alkali contents. We combine this new thermodynamic model with an empirical model for H_2O solubility from Lesne et al. (2011a) to yield a general model for H_2O–CO_2 solubility in mafic magmas called MafiCH.

1. The CO_2 model was calibrated using recent experiments on six compositions from Allison et al. (2019) as well as four additional compositions from the literature. Using multiple linear regression analysis, we have derived two empirical compositional relationships (Eqs. 6–7) that describe the thermodynamic parameters $\Delta V_r^{0,m}$ (partial molar volume change) and $\ln K_0$ (equilibrium constant at reference conditions).
2. The MafiCH model is calibrated for compositions with 44 to 53 wt% SiO_2 and 2 to 9 wt% total alkalis ($Na_2O + K_2O$), at pressures between ~ 50 and 700 MPa. A comparison with experimental data from magmas both within and beyond this compositional space suggests that MafiCH is very accurate within its calibrated range (i.e., mafic magmas with cation fractions within the ranges shown in Fig. 5). In some cases, MafiCH can be used beyond the calibrated compositional range, as long as the melt is a relatively depolymerized composition with CO_2 stored as CO_3.
3. One of the primary benefits of the MafiCH model is that it accurately describes CO_2 solubility behavior in mafic magmas at a range of crustal pressures. The CO_2 model is particularly robust because it is based in thermodynamics, calibrated across a wide P–X range of mafic magmas, and employs the full multicomponent magma composition to determine CO_2 solubility relationships.
4. The new MafiCH model yields melt inclusion saturation pressures that are typically lower than the pressures predicted by previously published volatile solubility models relevant to mafic magmas. The previously published models show the most divergence from MafiCH in less constrained compositional regions such as in magmas with higher SiO_2 contents (i.e., basaltic andesites), as well as magmas with relatively high (> 7 wt%) and low (< 3 wt%) total alkali contents. Many of the more recent models show similar trends in volatile solubility by magma composition, suggesting that models are beginning to agree on the elemental controls on volatile solubility.
5. Previously published volatile solubility models have developed compositional indices such as SiO_2, Π (or Π*) and NBO/O to describe solubility within restricted compositional regions. CO_2 solubility determined

using the MafiCH model does not directly correlate with any of these indices. However, the agpaitic index, $(Ca^{+2}+Na^{+1}+K^{1})/Al^{+3}$, does generally scale with CO_2 solubility calculated by the MafiCH model across a wide compositional range of mafic magmas. Additional analysis suggests that the influence of individual compositional components will be required to further improve volatile solubility models.

6. Based on calculations using the MafiCH model, Na^{+1} and Ca^{+2} appear to have the strongest positive effect on CO_2 solubility and Al^{+3} has a nearly equal negative effect. K^{+1} also has a strong positive effect. Other elements (e.g., Si^{+4}, Mg^{+2}) individually have little effect on CO_2 solubility in this compositional range.
7. The absolute solubility influence of each element varies depending on the abundance of other elements. This assessment suggests that the full multi-component magma composition is necessary to constrain CO_2 solubility for mafic magmas. It also suggests that additional experiments are required to constrain compositional regions that extend beyond the calibrated range of the MafiCH model.

Supplementary Information The online version contains supplementary material available at https://doi.org/10.1007/s00410-022-01903-y.

Acknowledgements This work was supported by NSF grants EAR-1322078 and EAR-1642569 to ABC and KR. Thanks to Mattia de' Michieli Vitturi for discussions regarding model calculators and James Thompson for help with Python. We are grateful to Kayla Iacovino and an anonymous reviewer for thoughtful comments that improved this manuscript, as well as Mark Ghiorso for editorial handling.

Author contributions All the authors conceptualized the project, interpreted the results, and edited the paper. CMA calibrated and tested the model, generated the excel calculator and python scripts, performed all calculations for the previously published models, and wrote the original draft of the paper.

Funding This work was supported by NSF grants EAR-1322078 and EAR-1642569 to ABC and KR.

Availability of data and materials No new data were collected for this study.

Code availability An excel spreadsheet and two python scripts are available in the supplementary material to perform calculations with the MafiCH model.

Declarations

Conflict of interest Not applicable.

References

Allison CM, Roggensack K, Clarke AB (2019) H_2O–CO_2 solubility in alkali-rich mafic magmas: new experiments at mid-crustal pressures. Contrib Mineral Petrol 174:58. https://doi.org/10.1007/s00410-019-1592-4

Baker MB, Grove TL (1985) Kinetic controls on pyroxene nucleation and metastable liquid lines of descent in a basaltic andesite. Am Mineral 70:279–287

Behrens H, Misiti V, Freda C, Vetere F, Botcharnikov RE, Scarlato P (2009) Solubility of H_2O and CO_2 in ultrapotassic melts at 1200 and 1250 degrees C and pressure from 50 to 500 MPa. Am Mineral 94:105–120. https://doi.org/10.2138/am.2009.2796

Berndt J, Liebske C, Holtz F, Freise M, Nowak M, Ziegenbein D, Hurkuck W, Koepke J (2002) A combined rapid-quench and H_2-membrane setup for internally heated pressure vessels: description and application for water solubility in basaltic melts. Am Mineral 87:1717–1726

Blank JG, Brooker RA (1994) Experimental studies of carbon dioxide in silicate melts: solubility, speciation, and stable carbon isotope behavior. In: Carroll MR, Holloway JR (eds) Volatiles in magmas, vol 30. Mineralogical Society of America, Washington, pp 157–186

Botcharnikov R, Freise M, Francois H, Behrens H (2005) Solubility of C-O-H mixtures in natural melts: new experimental data and application range of recent models. Annals of Geophys 48:633–646

Brooker RA, Kohn SC, Holloway JR, McMillan PF (2001) Structural controls on the solubility of CO_2 in silicate melts part I: bulk solubility data. Chem Geol 174:225–239

Cocheo PA (1994) The solubility of water in basanitic melts at low pressures, MS thesis. Arizona State University

Di Matteo V, Mangiacapra A, Dingwell DB, Orsi G (2006) Water solubility and speciation in shoshonitic and latitic melt composition from Campi Flegrei Caldera (Italy). Chem Geol 229:113–124. https://doi.org/10.1016/j.chemgeo.2006.01.015

Dixon JE (1997) Degassing of alkalic basalts. Am Mineral 82:368–378

Dixon JE, Stolper EM, Holloway JR (1995) An experimental study of water and carbon dioxide solubilities in mid ocean ridge basaltic liquids. Part I: calibration and solubility models. J Petrol 36(6):1607–1631

Duan X (2014) A general model for predicting the solubility behavior of H_2O–CO_2 fluids in silicate melts over a wide range of pressure, temperature and compositions. Geochim Cosmochim Acta 125:582–609. https://doi.org/10.1016/j.gca.2013.10.018

Duan Z, Zhang Z (2006) Equation of state of the H_2O, CO_2, and H_2O–CO_2 systems up to 10 GPa and 2573.15 K: molecular dynamics simulations with ab initio potential surface. Geochim Cosmochim Acta 70:2311–2324. https://doi.org/10.1016/j.gca.2006.02.009

Eguchi J, Dasgupta R (2018) A CO_2 solubility model for silicate melts from fluid saturation to graphite or diamond saturation. Chem Geol 487:23–38. https://doi.org/10.1016/j.chemgeo.2018.04.012

Fanara S, Botcharnikov RE, Palladino DM, Adams F, Buddensieck J, Mulch A, Behrens H (2015) Volatiles in magmas related to the Campanian Ignimbrite eruption: Experiments vs. natural findings. Am Mineral 100(10):2284–2297. https://doi.org/10.2138/am-2015-5033

Fine G, Stolper E (1986) Dissolved carbon dioxide in basaltic glasses: concentration and speciation. Earth Planet Sci Lett 76:263–278

Ghiorso MS, Gualda GAR (2015) An H_2O–CO_2 mixed fluid saturation model compatible with rhyolite-MELTS. Contrib Mineral Petrol 169:53. https://doi.org/10.1007/s00410-015-1141-8

Holloway JR (1977) Fugacity and activity of molecular species in supercritical fluids. In: Fraser DG (ed) Thermodynamics in geology. Reidel, Dordrect, pp 161–181

Holloway JR (1981) Volatile interactions in magmas. In: Newton RC, Navrotsky A, Wood BJ (eds) Thermodynamics of minerals and melts. Springer-Verlag, New York, pp 273–293

Holloway JR (1987) Igneous fluids. Rev Mineral Geochem 17(1):211–232

Holloway JR, Blank JG (1994) Application of experimental results to C-O-H species in natural melts. In: Carroll MR, Holloway JR (eds) Volatiles in magmas, vol 30. Mineralogical Society of America, Washington, pp 187–230

Iacono-Marziano G, Morizet Y, Le Trong E, Gaillard F (2012) New experimental data and semi-empirical parameterization of H_2O–CO_2 solubility in mafic melts. Geochim Cosmochim Acta 97:1–23. https://doi.org/10.1016/j.gca.2012.08.035

Iacovino K, Moore G, Roggensack K, Oppenheimer C, Kyle P (2013) H_2O–CO_2 solubility in mafic alkaline magma: applications to volatile sources and degassing behavior at Erebus volcano, Antarctica. Contrib Mineral Petrol 166:845–860. https://doi.org/10.1007/s00410-013-0877-2

Iacovino K, Oppenheimer C, Scaillet B, Kyle P (2016) Storage and evolution of mafic and intermediate alkaline magmas beneath Ross Island. Antarctica J Petrol 57(1):93–118. https://doi.org/10.1093/petrology/egv083

Iacovino K, Matthews S, Wieser PE, Moore GM, Bégué F (2021) VESIcal Part I: an open-source thermodynamic model engine for mixed volatile (H_2O-CO_2) solubility in silicate melts. Earth Space Sci 8(11):e2020EA001584. https://doi.org/10.1029/2020EA001584

Kilinc A, Carmichael ISE, Rivers ML, Sack RO (1983) The ferric-ferrous ratio of natural silicate liquids equilibrated in air. Contrib Mineral Petrol 83:136–140

Lesne P, Scaillet B, Pichavant M, Iacono-Marziano G, Beny JM (2011a) The H_2O solubility of alkali basalts: an experimental study. Contrib Mineral Petrol 162(1):133–151. https://doi.org/10.1007/s00410-010-0588-x

Lesne P, Scaillet B, Pichavant M, Beny JM (2011b) The carbon dioxide solubility in alkali basalts: an experimental study. Contrib Mineral Petrol 162(1):153–168. https://doi.org/10.1007/s00410-010-0585-0

Lowenstern JB (1995) Applications of silicate-melt inclusions to the study of magmatic volatiles. In: Thompson JFH (ed) Magmas, fluids and ore deposition. Mineralogical Association of Canada, Short Course 23, Quebec, pp 71–99

Mangan MT, Sisson TW, Hankins WB, Shimizu N, Vennemann T (2021) Constraints on deep, CO_2-rich degassing at arc volcanoes from solubility experiments on hydrous basaltic andesite of Pavlof Volcano, Alaska Peninsula, at 300 to 1200 MPa. Am Miner. https://doi.org/10.2138/am-2021-7531

Moore G, Vennemann T, Carmichael ISE (1995) Solubility of water in magmas to 2 kbar. Geology 23:1099–1102

Moore G, Vennemann T, Carmichael ISE (1998) An empirical model for the solubility of H_2O in magmas to 3 kilobars. Am Mineral 83:36–42

Mysen BO (1976) The role of volatiles in silicate melts: solubility of carbon dioxide and water in feldspar, pyroxene, and feldspathoid melts to 30 kb and 1625 °C. Am J Sci 276:969–996

Newman S, Lowenstern JB (2002) VOLATILECALC: a silicate melt-H_2O-CO_2 solution model written in Visual Basic for excel. Comput Geosci 28(5):597–604. https://doi.org/10.1016/S0098-3004(01)00081-4

Ohlhorst S, Behrens H, Holtz F (2001) Compositional dependence of molar absorptivities of near-infrared OH- and H_2O bands in rhyolitic to basaltic glasses. Chem Geol 174:5–20

Papale P (1997) Thermodynamic modeling of the solubility of H_2O and CO_2 in silicate liquids. Contrib Mineral Petrol 126:237–251

Papale P, Polacci M (1999) Role of carbon dioxide in the dynamics of magma ascent in explosive eruptions. Bull Volcanol 60:583–594

Papale P, Moretti R, Barbato D (2006) The compositional dependence of the saturation surface of H_2O+CO_2 fluids in silicate melts. Chem Geol 229:78–95. https://doi.org/10.1016/j.chemgeo.2006.01.013

Pichavant M, Di Carlo I, Le Gac Y, Rotolo SG, Scaillet B (2009) Experimental constraints on the deep magma feeding system at Stromboli volcano. Italy J Petrol 50(4):601–624. https://doi.org/10.1093/petrology/egp014

Pichavant M, Scaillet B, Pommier A, Iacono-Marziano G, Cioni R (2014) Nature and evolution of primitive Vesuvius magmas: an experimental study. J Petrol 55(11):2281–2310. https://doi.org/10.1093/petrology/egu057

Schanofski M, Fanara S, Schmidt BC (2019) CO_2–H_2O solubility in K-rich phonolitic and leucititic melts. Contrib Mineral Petrol 174:52. https://doi.org/10.1007/s00410-019-1581-7

Saxena SK, Fei Y (1987) High pressure and high temperature fluid fugacities. Geochim Cosmochim Acta 51:783–791

Shishkina TA, Botcharnikov RE, Holtz F, Almeev RR, Portnyagin MV (2010) Solubility of H_2O- and CO_2-bearing fluids in tholeiitic basalts at pressures up to 500 MPa. Chem Geol 277:115–125. https://doi.org/10.1016/j.chemgeo.2010.07.014

Shishkina TA, Botcharnikov RE, Holtz F, Almeev RR, Jazwa AM, Jakubiak AA (2014) Compositional and pressure effects on the solubility of H_2O and CO_2 in mafic melts. Chem Geol 388:112–129. https://doi.org/10.1016/j.chemgeo.2014.09.001

Stolper E, Holloway JR (1988) Experimental determination of the solubility of carbon dioxide in molten basalt at low pressure. Earth Planet Sci Lett 87:397–408

Thibault Y, Holloway JR (1994) Solubility of CO_2 in a Ca-rich leucitite: effects of pressure, temperature, and oxygen fugacity. Contrib Mineral Petrol 116:216–224

Vetere F, Botcharnikov RE, Holtz F, Behrens H, De Rosa R (2011) Solubility of H_2O and CO_2 in shoshonitic melts at 1250 °C and pressures from 50 to 400 MPa: implications for Campi Flegrei magmatic systems. J Volcanol Geotherm Res 202:251–261. https://doi.org/10.1016/j.jvolgeores.2011.03.002

Vetere F, Holtz F, Behrens H, Botcharnikov RE, Fanara S (2014) The effect of alkalis and polymerization on the solubility of H_2O and CO_2 in alkali-rich silicate melts. Contrib Mineral Petrol 167:1014. https://doi.org/10.1007/s00410-014-1014-6

Wieser PE, Iacovino K, Matthews S, Moore G, Allison CM (2022) A critical approach to volatile solubility modeling using the open-source engine VESIcal. Earth Space Sci. https://doi.org/10.1029/2021EA001932

Witham F, Blundy J, Kohn SC, Lesne P, Dixon J, Churakov SV, Botcharnikov R (2012) SolEx: a model for mixed COHSCl-volatile solubilities and exsolved gas compositions in basalt. Comput Geosci 45:87–97. https://doi.org/10.1016/j.cageo.2011.09.021